UCLA
UCLA Electronic Theses and Dissertations

Title
Nonlinear Model Reduction for Groundwater Flow and Solute Transport

Permalink
https://escholarship.org/uc/item/6kg0v9vj

Author
stanko, zachary p

Publication Date
2019

Peer reviewed|Thesis/dissertation

eScholarship.org Powered by the California Digital Library
University of California

UNIVERSITY OF CALIFORNIA

Los Angeles

Nonlinear Model Reduction for Groundwater Flow and Solute Transport

A dissertation submitted in partial satisfaction of the

requirements for the degree Doctor of Philosophy

in Civil Engineering

by

Zachary Stanko

2019

© Copyright by

Zachary Stanko

2019

ABSTRACT OF THE DISSERTATION

Nonlinear Model Reduction for Groundwater Flow and Solute Transport

By

Zachary Stanko

Doctor of Philosophy in Civil Engineering

University of California, Los Angeles, 2019

Professor William W. Yeh, Chair

Groundwater flow and solute transport models are necessary for understanding the quantity and quality of water in the subsurface. As these models get increasingly complex, their computational runtimes often increase. Reduced models can be developed to approximate the full complex model with reasonable accuracy and shorter runtimes. In this research, proper orthogonal decomposition (POD) is used to identify a lower dimensional subspace that captures most of the information contained in the full model system. Then, because of the nonlinearities present in many flow and transport models, a discrete empirical interpolation method (DEIM) is used to identify an additional lower dimensional subspace that captures the nonlinear dynamics. The reduced modeling framework is implemented within the MODFLOW and MT3DMS software families for groundwater flow and solute transport, respectively. The combined POD-DEIM approach is first applied to an unconfined groundwater flow model where dimensions

were reduced by two and three orders of magnitude. The same approach is then applied to a solute transport model simulating nonlinear sorption where dimensions were also reduced by two and three orders of magnitude. The reduced models performed with sufficient accuracy and faster runtimes. The faster runtimes could allow for the reduced models to be embedded into an optimization or uncertainty analysis where thousands to millions of model runs could be required. With the developed POD-DEIM approach, reduced modeling is now viable for any existing MODFLOW or MT3DMS model.

The dissertation of Zachary Stanko is approved.

Mekonnen Gebremichael

Steven A. Margulis

Lieven Vandenberghe

William W. Yeh, Committee Chair

University of California, Los Angeles

2019

DEDICATION

This dissertation is dedicated to my family.

Especially to my father, Ken Stanko, for always supporting me and encouraging me to follow my own path. Rest in peace.

TABLE OF CONTENTS

LIST OF FIGURES viii

LIST OF TABLES xii

ACKNOWLEDGMENTS xiv

VITA xvi

1. Introduction 1

    1.1. Groundwater 1

    1.2. Groundwater Modeling 1

    1.3. Model Reduction 3

    1.4. Modeling Software 4

    1.5. References 5

2. Nonlinear model reduction of unconfined groundwater flow using POD and DEIM (reprint) 6

    2.1. Introduction 6

    2.2. Methods 7

    2.3. Results 11

    2.4. Discussion 16

    2.5. Conclusion 19

    2.6. References 19

3. Nonlinear model reduction of solute transport models (reprint) 20

3.1. Introduction.....20

3.2. Methodology.....21

3.3. One-dimensional test case 24

3.4. Two-dimensional test case.....26

3.5. Discussion.....29

3.6. Conclusion 33

3.7. References.....34

4. Conclusion 35

4.1. Reduced Nonlinear Groundwater Flow 35

4.2. Reduced Nonlinear Solute Transport.....35

4.3. Overall Conclusions.....36

5. Future Research 37

5.1. Optimal Snapshot Selection.....37

5.2. Coupled Flow and Transport 38

5.3. More Complex Applications.....39

5.4. Software Packages 39

5.5. References.....40

LIST OF FIGURES

Chapter 2 Figures

2.1. Algorithm for selecting the interpolation indices z_j for $j=1,\ldots,d$.....9

2.2. The flow chart describes the process of collecting snapshots for both traditional POD and DEIM; constructing the snapshot sets and obtaining the bases; and solving with the POD-DEIM reduced model.....10

2.3. The 1-dimensional model shows the conductivity zones and the water table after 30 days of pumping, creating the unconfined conditions, for pumping rates of 100 and 200 m^3/day 11

2.4. The domain of the 2D test case is shown with a model grid of 198 rows and 198 columns and six conductivity zones that span several orders of magnitude. There are five wells that pump at various rates and head-dependent features (river and drain) are included 12

2.5. (left) The results from the 1-D test are shown as a residual between full model head and reduced model head, for each of the 90 time steps in the POD-DEIM reduced model. (right) A cross-section of head also shows a match between the full and reduced models.....13

2.6. (left) The error in the nonlinear approximation is shown to be at a maximum where the well is located, cell 107, and at the beginning of each time step. (right) A time series of head at the well is also shown above a time series of nonlinear error at the well.....13

2.7. The RMSE in head for each model cell is calculated over all time steps and shown over the model domain with DEIM interpolation points shown as red dots. (a) Errors in h and (b) errors in Ah for the reduced model with d=200 are shown. Also shown are the (c) errors in in h and (d) errors in Ah for the reduced model with d=250 14

2.8. The water table drawdown in selected regions is shown for the Full and POD-DEIM reduced model. Cross sections are shown for (a) 305 days at Well 3; (b) 305 days at Well 2; (c) 395 days at Well 1; and (d) 395 days at Well 2 15

2.9. (top) The absolute error in head, as well as (bottom) the error in the nonlinear approximation, is shown for (left) day 305 and (right) day 395, times when large errors were observed and the end of the recovery period 16

2.10. Absolute error at the location found to have the largest error for the (a) POD, (b) POD-DEIM$_{200}$, and (c) POD-DEIM$_{250}$ reduced models. The MAE for the entire domain is computed for each time step and shown as a time series 17

2.11. A comparison of the RMSE for the residual error in head ($|h-h_r|$) for each of the reduced models, POD, POD-DEIM$_{200}$, POD-DEIM$_{225}$, and POD-DEIM$_{250}$ when measured against the full model 18

Chapter 3 Figures

3.1. The 1D test case full model solute concentrations after 100 days.....25

3.2. A heatmap to show the combinatorial search over the two reduced dimensions, r, and d, with color representing the maximum error between the full model and the reduced model with each unique combination of reduced dimensions. 25

3.3. The accuracy of the reduced model with respect to the full model for concentration breakthrough curves at x=20, x=40, x=60, and x=80 26

3.4. The POD-DEIM (r=18, d=42) reduced model error shown for absolute error over all time (left) and by comparing simulated concentrations for the full and reduced model at snapshots for 50 days (top right) and 100 days (bottom right) 26

3.5. a) The 2-D model domain showing the concentration plume after 5,000 days (MODFLOW well cells shown in blue; constant head cells in green; and drain cells in purple) and b) the contours of hydraulic head and the randomly generated hydraulic conductivity (K) field 27

3.6. An abbreviated search over the reduced dimension space to find appropriate combinations of dimensions p and d 29

3.7. Contours of concentration (g/m3) at the end of the simulation (5,000 days) for the full model (solid lines) and the POD-DEIM reduced model (dotted

lines). MODFLOW wells are shown as blue rectangles and concentration observation locations as red diamonds 30

3.8. Concentration breakthrough curves at three observation locations for both the full model and the POD-DEIM reduced model with the (row, column) location of the observation.....30

3.9. The RMSE of the concentration snapshots for the POD-DEIM reduced model 31

3.10. The NRMSE of the nonlinear snapshots for a POD-DEIM reduced model with 286 interpolation points (shown as black dots) 32

3.11. a) The percent exceedance for the RMSE of the entire model domain at each snapshot time for each of the 50 samples; and b) The maximum error in concentration for each of the 50 samples as a function of the maximum simulated concentration.....33

LIST OF TABLES

Chapter 2 Tables

2.1. Variable symbols and definitions along with appropriate units and initial default values 8

2.2. Parameter and pumping values for the 2D test case 10

2.3. Model reduction results are displayed in comparison to the full, unreduced model.....12

2.4. Hydraulic head error statistics over 50 random samples for each of the 2D reduced models 17

2.5. Nonlinear error statistics over 50 random samples for each of the 2D reduced models 18

Chapter 3 Tables

3.1. Variable symbols and definitions along with appropriate units 22

3.2. The values assigned to the 1-D MT3D-USGS transport model and the MODFLOW groundwater model.....24

3.3. Various error metrics compared for the POD (r=18) and the POD-DEIM (r=18, d=42) reduced models. Minimum and maximum concentrations, absolute errors as defined by the full model minus the reduced model, root mean squared error (RMSE), and normalized root mean squared

error (NRMSE), are all within acceptable values. All units are g/m^3 except NRMSE, which is dimensionless 26

3.4. The values assigned to the 2-D MT3D-USGS transport model and the MODFLOW groundwater model.....28

3.5. Error statistics for the single reduced model (with mass loading of 1,250 g/day) and 50 samples of reduced models with random mass loading rates.....31

ACKNOWLEDGMENTS

Primarily, I would like to thank William W-G. Yeh for all the support over the years. This research would not be possible without his guidance or his trust in me as a researcher. Thank you Dr. Yeh, for the fortunate opportunity to work with you, for the many lessons I've learned, and for the honor to publish this research.

I also have a debt of gratitude for my professors at Humboldt State University. To Eileen Cashman, Brad Finney, Arne Jacobson, Margaret Lang, and Robert Willis: Thank you for encouraging me throughout my time at HSU and for believing in me before I believed in myself.

An additional thank you goes to Tracy Nishikawa and Claudia Faunt of the USGS. Thanks for allowing me to work on challenging and rewarding projects while I was often busy at school. I do not think I could have finished this work without the flexibility and patience you've shown for me.

Many thanks as well to Scott Boyce and Adam Siade who both mentored me as a new graduate student and as a new USGS employee. Starting something new and difficult was a little less intimidating with friends like these who had taken similar steps before me and were willing to share their experience.

Lastly, a huge thank you to the life-long friends I have who were always kind when I needed kindness and honest when I needed honesty. Your friendships mean the world to me.

This material is based on work supported by NSF under award EAR-1314422. Partial support also was provided by an AECOM endowment.

Chapter 2 contains the following reprinted journal article:

> Stanko, Z. P., Boyce, S. E., & Yeh, W. W.-G. (2016). Nonlinear model reduction of unconfined groundwater flow using POD and DEIM. Advances in Water Resources, 97, 130–143. https://doi.org/10.1016/j.advwatres.2016.09.005

and retains the following copyright:

> © 2016. Made available under the CC-BY-NC-ND 4.0 license
> http://creativecommons.org/licenses/by-nc-nd/4.0/

Chapter 3 contains the following reprinted journal article:

> Stanko, Z. P., & Yeh, W. W.-G. (2019). Nonlinear model reduction of solute transport models. Advances in Water Resources, 130, 157–171. https://doi.org/10.1016/j.advwatres.2019.05.028

and retains the following copyright:

> © 2019. Made available under the CC-BY-NC-ND 4.0 license
> http://creativecommons.org/licenses/by-nc-nd/4.0/

VITA

2000	Fox Chapel Area High School Pittsburgh, Pennsylvania
2006	B.S., Mathematics University of Pittsburgh
2012	B.S., Environmental Resources Engineering Humboldt State University
2016	M.S. Civil Engineering University of California, Los Angeles
2012-present	Hydrologist, United States Geological Survey: California Water Science Center San Diego, CA

SELECTED PUBLICATIONS AND PRESENTATIONS

Xu, B., Zhong, P.-A., Stanko, Z., Zhao, Y., & Yeh, W. W.-G. (2015). A multiobjective short-term optimal operation model for a cascade system of reservoirs considering the impact on long-term energy production. Water Resources Research, 51(5), 3353–3369. https://doi.org/10.1002/2014WR015964

Stanko, Z. P., Boyce, S. E., & Yeh, W. W.-G. (2016). Nonlinear model reduction of unconfined groundwater flow using POD and DEIM. Advances in Water Resources, 97, 130–143. https://doi.org/10.1016/j.advwatres.2016.09.005

Stanko, Z. P., & Yeh, W. W.-G. (2019). Nonlinear model reduction of solute transport models. Advances in Water Resources, 130, 157–171. https://doi.org/10.1016/j.advwatres.2019.05.028

Nishikawa, T., ed. (2018). Santa Barbara and Foothill groundwater basins Geohydrology and optimal water resources management—Developed using density dependent solute transport and optimization models, U.S. Geological Survey, Scientific Investigations Report 2018-5059, 4 chap. (A–D), variously paged, https://doi.org/10.3133/sir20185059

Stanko, Z. P., Fienen, M. N., & Faunt, C. C. (2017). Metamodel analysis of California's coastal groundwater basins to identify undesirable results of management actions. In Proceedings of the MODFLOW and More 2017 Conference. Golden CO.

1 Introduction

1.1 Groundwater

Fresh groundwater is a valuable resource throughout the world. Water supply from groundwater is vital to municipal, agricultural, and industrial uses. Without an adequate understanding of the available water, and the quality of that water, aquifers can become irreversibly damaged. Damages range from chronic lowering of water levels, which can lead to compaction of the porous media and reduced storage capacity, to depleted surface water bodies that depend on groundwater interaction for a balanced ecosystem. To mitigate these damages, water system managers are tasked with meeting the demands from conjunctive uses while developing sustainable practices. Sustainability is necessary to ensure that the quantity and quality of water can me maintained through periods of extreme climates, such as droughts. Since all plant and animal ecosystems throughout the biosphere depend on groundwater to some extent, the civilizations that impact this resource for other purposes have a duty to consider the long-term effects of their actions. Since groundwater resides in the subsurface and cannot be monitored easily, additional tools are needed to assess the state of the groundwater system.

1.2 Groundwater Modeling

Numerical modeling of groundwater allows for predictions of a system state in a subsurface environment. The models are derived from partial differential equations that govern the physical flow and chemical transport of substances in a porous media. The governing equations are comprised of state variables that describe the space- and time-dependent characteristics of the water system (water levels or concentration, for example); parameters that describe physical,

chemical or numerical properties; and variables that represent boundary conditions, initial conditions, and sources or sinks of a conserved substance. Solutions to these equations often require a numerical method. Frequently, the parameters used in the governing equations need to be estimated by some systematic approach. Precise values of these parameters can seldom be known so statistical methods are usually employed. Making predictions from numerical models is challenging because assumptions implicit in the equations and errors in the numerical implementation can lead to high uncertainty in the solutions. Prediction uncertainty can be addressed by using methods that require many model runs of different parameter combinations, possibly with multiple environmental or management scenarios.

Applications of groundwater models vary based on many factors but predictions of some kind are usually desired. Simulations of aquifers, or aquifer systems, can be used to evaluate current and future groundwater availability within a basin or watershed. The simulations often require many additional model runs—beyond those needed to estimate the parameters and address the uncertainty in the solutions—to sufficiently answer the questions posed by the stakeholders. For example, optimization methods are used to assess the best possible predicted outcomes under a range of management decisions and variable/parameter combinations. For model applications to sufficiently represent the real world, models tend towards higher complexity. Complexity arises when models include nonlinear relationships, discontinuous structural features, finer space and time considerations, larger model domains, and longer time horizons. These added complexities usually make each individual model run take longer to execute, computationally. For predictions that require optimization or statistical uncertainty analysis, models may need to be executed

thousands, even millions of times. Under computational resource limitations, some of these methods can be practically unrealistic or infeasible.

1.3 Model Reduction

Smaller, faster models are desired if thousands of model runs are needed but time and computer resources are limited. A broad field of research exists for the development of fast surrogate models, also known as model emulators, to replace a larger, complex simulation model, often referred to as the full model. Reduced models are a class of surrogate models that rely on projection methods to identify a basis of lower dimension that captures most of the information contained in the full model. Other types of surrogate models are data-driven and only consider model inputs and model outputs. One of the main advantages of a reduced model is that the physics used to develop the governing equation is represented in the reduced basis. It can be argued that methods that incorporate the physics are more robust with respect to changes in any system state. Regardless of the type of model emulator that is used, the goal remains the same: approximate the solution of the full model in a fraction of the time needed to run the full model.

Model reduction techniques vary in the groundwater modeling field depending on the type of full model that is approximated (i.e., reduced). Proper orthogonal decomposition (POD) is one of the more prevalent techniques. Studies using POD to reduce groundwater models are mostly limited to full models that are linear with respect to the state variables. When nonlinearities are present in the governing equation, strictly POD methods either decrease in their effectiveness (because reduced models still have calculations that scale with the full dimension) or cannot be used at all (because reduced models have errors that are too high). Enhancements to POD-based methods have been made for nonlinear applications in other fields. The discrete empirical interpolation

method (DEIM) has been developed to overcome the deficiencies of POD-only reduced models for nonlinear applications. The interpolation scheme ensures that the reduced model's calculations scale in size with the reduced dimensions only and that the reduced model's solutions approximate the full nonlinear solution more accurately. The speed and accuracy of a combined POD and DEIM approach is promising for nonlinear groundwater flow and solute transport, but it had yet to be demonstrated.

1.4 Modeling Software

There are many options when it comes to choosing the groundwater model software to use for a particular study. One option is to develop the code from scratch. This has benefits because the code can be designed for the exact purpose of the study without any additional bloat that can make published software very cumbersome to work with. The cost to this approach is primarily that code developed by a researcher does not have the same level of trust, reliability, validity, and flexibility that most formally developed modeling software has. If a proposed method is to be applied in any real-world setting and used for real-world planning and management this cost can outweigh the benefit. For this reason, a reliable software was chosen for the implementation of the methods in this study.

The USGS-developed MODFLOW-2005 (Harbaugh, 2005) and MODFLOW-related software are widely used for groundwater modeling internationally. There are a range of feature packages that can be used to simulate a variety of physical processes and structural components within a groundwater basin. If a model reduction algorithm were implemented within MODFLOW, it would allow for a wide array of applications. Any existing and future MODFLOW models could have the means of developing a reduced version. The solute transport code that is compatible

with MODFLOW and has seen many international applications is MT3DMS (Zheng and Wang, 1999), which has been updated recently into a version called MT3D-USGS (Bedekar et al., 2016). Similarly, a model reduction routine within this code would have much interest. Since the modeling framework is consistent between MODFLOW and MT3D-USGS, the model reduction component can be integrated into both software in a similar manner.

1.5 References

Bedekar, Vivek, Morway, E.D., Langevin, C.D., and Tonkin, Matt (2016), MT3D-USGS version 1: A U.S. Geological Survey release of MT3DMS updated with new and expanded transport capabilities for use with MODFLOW: U.S. Geological Survey Techniques and Methods 6-A53, 69 p., http://dx.doi.org/10.3133/tm6A53.

Harbaugh, A.W., 2005, MODFLOW-2005, The U.S. Geological Survey modular ground-water model—the Ground-Water Flow Process: U.S. Geological Survey Techniques and Methods 6-A16, variously p.

Zheng, C., Wang, P.P. (1999). MT3DMS: A Modular Three-Dimensional Multispecies Transport Model for simulation of advection, dispersion and chemical reactions of contaminants in groundwater systems. 239 p.

Advances in Water Resources 97 (2016) 130–143

Contents lists available at ScienceDirect

Advances in Water Resources

journal homepage: www.elsevier.com/locate/advwatres

Nonlinear model reduction of unconfined groundwater flow using POD and DEIM

Zachary P. Stanko[a], Scott E. Boyce[b,1], William W.-G. Yeh[a,*]

[a] Department of Civil and Environmental Engineering, University of California, Los Angeles, CA 90095, USA
[b] California Water Science Center, U.S. Geological Survey, 4165 Spruance Rd., Suite 200, San Diego, CA 92101-0812, USA

ARTICLE INFO

Article history:
Received 14 February 2016
Revised 29 July 2016
Accepted 12 September 2016
Available online 13 September 2016

Keywords:
Model reduction
Unconfined flow
Proper orthogonal decomposition
Discrete empirical interpolation method
Nonlinear differential equations

ABSTRACT

Nonlinear groundwater flow models have the propensity to be overly complex leading to burdensome computational demands. Reduced modeling techniques are used to develop an approximation of the original model that has smaller dimensionality and faster run times. The reduced model proposed is a combination of proper orthogonal decomposition (POD) and the discrete empirical interpolation method (DEIM). Solutions of the full model (snapshots) are collected to represent the physical dynamics of the system and Galerkin projection allows the formulation of a reduced model that lies in a subspace of the full model. Interpolation points are added through DEIM to eliminate the reduced model's dependence on the dimension of the full model. POD is shown to effectively reduce the dimension of the full model and DEIM is shown to speed up the solution by further reducing the dimension of the nonlinear calculations. To show the concept can work for unconfined groundwater flow model, with added nonlinear forcings, one-dimensional and two-dimensional test cases are constructed in MODFLOW-OWHM. POD and DEIM are added to MODFLOW as a modular package. Comparing the POD and the POD-DEIM reduced models, the experimental results indicate similar reduction in dimension size with additional computation speed up for the added interpolation. The hyper-reduction method presented is effective for models that have fine discretization in space and/or time as well as nonlinearities with respect to the state variable. The dual reduction approach ensures that, once constructed, the reduced model can be solved in an equation system that depends only on reduced dimensions.

© 2016 Published by Elsevier Ltd.

1. Introduction

Reduced modeling has become a necessary field of research given the near-complete scientific understanding of many physical processes and the ensuing complexity of mathematical models. Reduced modeling techniques are commonly applied to decrease the computational burden associated with high dimensionality. Traditionally, the proper orthogonal decomposition (POD) method is used to formulate a low dimension basis for high-dimension dynamical systems (Vermeulen et al., 2004; Antoulas et al., 2001). The key advantage of using POD for model reduction is that the reduced model maintains the physics of the full model and captures the dominating characteristics of the full model. Applications of POD is also known in the literature as Empirical Orthogonal Functions (EOF) (von Storch and Hannoschöck, 1985; McPhee and Yeh, 2008), Coherent Structures (CS) (Sirovich, 1987), Principal Component Analysis (PCA), Karhunen-Loéve (KL) methods (Graham and Kevrekidis, 1996), or Common Factor Analysis (CFA) (Reyment and Joreskog, 1993).

For groundwater flow specifically, most previous applications of POD have utilized the confined flow equation, which is linear with respect to the state variable of interest, namely, the hydraulic head (Boyce and Yeh, 2014). To briefly describe this reduced model construction: one selects a set of model simulation results at specific instances of simulation time, which is called a snapshot set. POD is then applied to identify the singular values of the matrix composed of the snapshots. Only a selected few of the singular values are chosen such that most of the variance of the original system is retained. A subspace basis is then constructed and Galerkin projection is applied to form the reduced model (Vermeulen et al., 2004). Extensions to this method for nonlinear problems include modifications to the Galerkin projection—such as using a Petrov–Galerkin projection for stabilization (Ştefănescu et al., 2015) or adaptive Ritz vectors (Nigro et al., 2015)—or alternate strategies such as minimization of the L^1 norm representing the reduced model approximation error (Abgrall and Amsallem, 2016). Alternatively, linearization techniques such as quasilinearization, can be utilized to

* Corresponding author.
E-mail address: williamy@seas.ucla.edu (W.W.-G. Yeh).
[1] Formerly at University of California, Los Angeles, USA.

http://dx.doi.org/10.1016/j.advwatres.2016.09.005
0309-1708/© 2016 Published by Elsevier Ltd.

facilitate POD reduced model construction for the case of nonlinear parameter estimation (Siade et al., 2012).

While confined flow models have nice linear properties that allow for flexible manipulation and superposition, nonlinearities are unavoidable in many groundwater modeling projects. Requiring unconfined flow creates nonlinear equations that are harder to solve and hence more difficult to reduce successfully. Nonlinear model reduction has been addressed thoroughly in (Cardoso et al., 2009), where a Markov chain Monte Carlo simulation was performed for an inverse problem utilizing Bayesian inference. Boyce et al. (2015) also successfully reduced an unconfined groundwater model using the Newton formulation of MODFLOW, MODFLOW-NWT (Niswonger et al., 2011). These examples of successful groundwater model reduction with reduced basis methods illustrate the added difficulty with nonlinearities and present methods that are only applicable in unique contexts. That is, the solution scheme in both studies involves Newton's method which requires approximation of a Jacobian that may not be easy to obtain. Also, approximating the Jacobian and formulating Newton's method can effectively linearizes the system since the Jacobian can be evaluated at prior values of head. Lastly, there are more inherent memory requirements for a Newton solution than the traditional MODFLOW (exactly twice as much), which may restrict large-scale applications (Niswonger et al., 2011).

The discrete empirical interpolation method (DEIM) is an effective approach to nonlinear approximations. Originally developed as the empirical interpolation procedure (EIP) (Barrault et al., 2004), with the discrete form introduced in (Chaturantabut and Sorensen, 2010). It has been used in conjunction with POD for reducing FitzHugh–Nagumo equations (Chaturantabut and Sorensen, 2010), shallow water equations (Ştefănescu and Navon, 2013), and an advection–diffusion–reaction system (Cardoso et al., 2009). These model reduction procedures are also called reduced basis (RB) methods and an EIP has been developed in this context by (Drohmann et al., 2012). Successful applications of RB methods to various forms of the Navier–Stokes equations (both steady and unsteady) are demonstrated to have significant computational advantages (Quarteroni and Rozza, 2007).

The joint application of POD and DEIM is a form of hyper-reduction for nonlinear equations. This type of model reduction in the literature of other fields is also gaining popularity. In electrical engineering, the methods have been successfully applied to a magnetostatic problem coupled to an electric circuit (Henneron and Clenet, 2014) and in mechanical engineering, the methods were used for a solid mechanics problem involving nonlinear elasticity (Radermacher and Reese, 2015). However, unconfined groundwater flow models have not yet been reduced in this manner. In this study, we propose a combined model reduction approach that: (1) performs POD on an unconfined groundwater flow model; (2) applies DEIM to the nonlinear component of the governing equation; and (3) implements the procedure within MODFLOW.

By enabling model reduction within MODFLOW, a very large assortment of existing MODFLOW models—many have single run times on the order of hours or even days—can be reduced to increase computational efficiency. Reducing the dimension of these models would permit large-scale applications—such as multi-objective optimization (Reed et al., 2013) or Monte Carlo uncertainty analysis (Kasprzyk et al., 2009; Tonkin and Doherty, 2009; Siade et al., 2015)—that can require hundreds of thousands, or even millions of groundwater model runs.

More robust reduced modeling techniques are needed for nonlinear dynamics in groundwater flow. Methods developed previously have resorted to using strategies designed for linear equations and do not address the additional time required to solve a system of nonlinear equations. In large-scale simulations, having nonlinear calculations that still have the computational complexity of the full model dimension greatly inhibits the value of developing the reduced model, which can have significant overhead itself. Application of POD-DEIM to the unconfined groundwater flow equations presents an opportunity to develop a hyper-reduced model utilizing controllable accuracy and computer runtimes that scale with reduced dimensions only.

2. Methods

The following methodology introduces unconfined groundwater flow equations and expands upon recent developments in POD and DEIM reduced modeling. The implementation of these methods within the commonly used MODFLOW software will be described. All variable definitions are compiled in Table 1 with the following convention: uppercase letters for scalar variables; bold lowercase for one-dimensional vectors; bold uppercase for two-dimensional matrices.

2.1. Unconfined groundwater flow

The general three-dimensional governing equation for constant-density groundwater flow in an unconfined aquifer is given by (Keating and Zyvoloski, 2009):

$$\nabla \cdot (\boldsymbol{K}\boldsymbol{h}\nabla \boldsymbol{h}) \pm \boldsymbol{q} = S_y \frac{\partial \boldsymbol{h}}{\partial t} \tag{1}$$

where $\nabla \bullet$ is the divergence operator, ∇ is the gradient operator, K is the isotropic hydraulic conductivity tensor [L/T], $\boldsymbol{h}$ is the hydraulic head [L], $\boldsymbol{q}$ is a volumetric flux per unit volume in or out of the system [L/T], t is the time [T], and S_y is the specific yield [−]. For the case of a two-dimensional flow and under the Dupuit assumptions (essentially horizontal flow), the governing equation for an unconfined aquifer then becomes the Boussinesq equation (Willis and Yeh, 1987):

$$\frac{\partial}{\partial x}\left[K_{xx}h\frac{dh}{dx}\right] + \frac{\partial}{\partial y}\left[K_{yy}h\frac{dh}{dy}\right] \pm W = S_y\frac{\partial h}{\partial t} \tag{2}$$

where K_{xx} and K_{yy} are the hydraulic conductivity parameters assumed to align with the x and y, and coordinates, respectively. In this case, W is the net source/sink into the aquifer (including areal recharge and point source wells) [$\mathrm{L\,T^{-1}}$]. Note that Eq. (2) is nonlinear as it involves the product terms of the state variable h.

Applying a finite difference approximation scheme to the spatial variables (x, y) yields the following system of nonlinear ordinary differential equations, represented in matrix form as Eq. (3):

$$\boldsymbol{A}\boldsymbol{h} + \boldsymbol{f} = \boldsymbol{B}\frac{d\boldsymbol{h}}{dt} \tag{3}$$

where $\boldsymbol{A}, \boldsymbol{B} \in \mathbb{R}^{n\times n}$ and $\boldsymbol{h}, \boldsymbol{f} \in \mathbb{R}^{n\times 1}$, n being the number of finite difference nodes on the model domain. $\boldsymbol{A}$ contains all coefficients of head that are internally calculated as functions of head at each time step, making the product term ($\boldsymbol{A}\boldsymbol{h}$) nonlinear. $\boldsymbol{B}$ contains constant coefficients for the temporal head change and constant spatial discretization values and $\boldsymbol{f}$ contains all head-independent sources or sinks of water and head-independent boundary conditions. The head at any time is then calculated using a backward-difference approach to ensure stability. After reordering some terms and multiplying through by −1, the following matrix equation (Eq. (4)) is calculated to represent the flow system at each time step:

$$\left[\frac{\boldsymbol{B}}{\Delta_t} - \boldsymbol{A}\right]\boldsymbol{h}^{t+1} = \frac{\boldsymbol{B}}{\Delta_t}\boldsymbol{h}^{t} + \boldsymbol{f}$$

Or

$$\boldsymbol{A}_h\boldsymbol{h}^{(t+1)} = b \tag{4}$$

Table 1
Variable symbols and definitions along with appropriate units and initial default values.

Symbol	Dimension	Units	Description
$\boldsymbol{h}$	$n \times 1$	[m]	Vector of groundwater head
$\boldsymbol{A}_h$	$n \times n$	[–]	Matrix containing nonlinear coefficients for the groundwater flow equation (elements that are functions of head)
$\boldsymbol{B}$	$n \times n$		Matrix containing linear coefficients for the groundwater flow equation (elements that are not a function of head)
$\boldsymbol{b}$	$n \times 1$	[–]	Right-hand side vector of the groundwater flow equation
K	Scalar	[m/day]	Hydraulic conductivity in the x and y principal directions
$\boldsymbol{q}$	$n \times 1$	[m/day]	Sources/sinks of water in flow per unit volume
S_y	Scalar	[–]	Specific yield coefficient
$\varepsilon_{\max}$	Scalar	[m]	Maximum difference in head in two consecutive iterations.
i, j			Indices for the model cells in the x and y direction
k			Index for the iteration of the nonlinear solver
t			Index for the model time steps
n	Scalar	[–]	Number of finite difference cells of the model domain
r	Scalar	[–]	Number of singular values retained from POD to create the reduced model
s	Scalar	[–]	Number of snapshots taken of the full model
d	Scalar	[–]	Number of interpolation points used for the POD-DEIM reduced model
Δ_t	Scalar	[days]	Uniform time step length
$\boldsymbol{\Phi}_h$	$s \times n$		Snapshot set of h
$\boldsymbol{\Phi}_b$	$s \times n$		Snapshot set of b
σ_i	Scalar		The ith singular value
$\mathbf{P}$	$n \times r$		Projection matrix formed from POD on Φ_h
$\mathbf{D}$	$n \times d$		Projection matrix formed from POD on Φ_d
$\mathbf{Z}$	$n \times d$		Permutation matrix to select the dominant rows of the system
z_j	Scalar		The jth interpolation index
$\boldsymbol{c}$	$d \times 1$		Vector of reduced variables in DEIM formulation
$\boldsymbol{h_r}$	$r \times 1$		Vector of state variables in the reduced space
$\boldsymbol{z}$	$d \times 1$		Vector of interpolation indices

Defining $[\frac{\boldsymbol{B}}{\Delta_t} - \boldsymbol{A}]$ as the nonlinear system matrix, $\boldsymbol{A}_h$, and $[\frac{\boldsymbol{B}}{\Delta_t}\boldsymbol{h}^t + \boldsymbol{f}]$ as the right hand side vector of constants, $\boldsymbol{b}$. A variety of indirect methods can be used to solve for $\boldsymbol{h}^{t+1}$ at each time step. For the full model, the current study utilizes the preconditioned conjugate-gradient solver (PCG), documented in (Hill, 1990) and Picard iteration for every time step, stopping when $\max_{1<i<n}(h_i^k - h_i^{k+1}) \leq \varepsilon_{max}$ (the maximum head difference from iteration k to $k+1$ is sufficiently small) or $\max_{1<i<n}(inflow_i^{k+1} - outflow_i^{k+1}) \leq r_{max}$ (the maximum flow residual is sufficiently small). These methods are already programmed into MODFLOW and the recently updated MODFLOW-OWHM (Hanson et al., 2014), which served as the base code for the POD-DEIM development and includes the Newton Formulation of MODFLOW. Eq. (4), which is called the full model, lies in the dimension $n \times n$, since there are n equations and n unknowns.

2.2. POD

A brief derivation of POD begins by approximating $\boldsymbol{h}^{t+1}$ with $\boldsymbol{P}\boldsymbol{h}_r^{t+1}$. The matrix $\boldsymbol{P} \in \mathbb{R}^{n \times r}$ is generated by applying singular value decomposition (SVD) on $\boldsymbol{\Phi}_h \in \mathbb{R}^{n \times s}$, a matrix composed of a set of simulated values of $\boldsymbol{h}$, called solution snapshots, for s selected time steps. $\boldsymbol{h}_r \in \mathbb{R}^{r \times 1}$ is then a reduced vector of dependent variables, where $r \ll n$ is chosen based in the r largest singular values (σ) of $\boldsymbol{\Phi}_h$ that account for nearly all (e.g., 99.99% or 99.999%) of the matrix's embedded information, called percent energy. An error threshold of percent energy ($\varepsilon_{\text{energy}}$) is used to specify the amount of information retained in the reduced basis

$$Percent\ Energy = \frac{\sum_{i=1}^{r}\sigma_i}{\sum_{i=1}^{rank(\boldsymbol{\Phi}_h)}\sigma_i} \times 100 \geq \varepsilon_{energy}.$$

Galerken Projection is then used to project the full model space onto a reduced subspace by pre-multiplying both sided by $\boldsymbol{P}^T$, resulting in Eq. (5). This process is described more thoroughly in Vermeulen et al. (2004) and as applied to a newton formulation of MODFLOW in Boyce et al. (2015). Eq. (5) is called the POD-reduced model and still requires matrix multiplication with a dimension of n when $\boldsymbol{P}^T\boldsymbol{A}_h$ is computed at each time step. Due to nonlinearities, each element of $\boldsymbol{A}_h$ must be recomputed each time step; an operation that also scales with n.

$$\boldsymbol{P}^T\boldsymbol{A}_h\ \boldsymbol{P}\boldsymbol{h}_r^{t+1} = \boldsymbol{P}^T\boldsymbol{b} \tag{5}$$

2.3. DEIM

The discrete empirical interpolation method is implemented specifically to reduce the nonlinear term's dependency on the full dimension of the original model. At each time step, it may be computationally burdensome and unnecessary to compute any nonlinear approximations in the POD formulation using the full system's state space. To approximate nonlinearities in a reduced space, the nonlinear term is evaluated at selected interpolation points. The nonlinear projection basis is obtained via POD on snapshots of the nonlinear components only. The initial DEIM approximation (Eq. (6)) is made by approximating the nonlinear operation ($\boldsymbol{A}_h\boldsymbol{h}^{t+1}$) with a linear interpolation. The selection algorithm for the interpolation indices chooses points that have the largest residual error when iteratively approximating the nonlinear term with basis vectors (selected columns of $\boldsymbol{D}$) times a vector of new reduced variables, $\boldsymbol{c}$.

$$\boldsymbol{A}_h\boldsymbol{h}^{t+1} \cong \boldsymbol{D}\boldsymbol{c} \tag{6}$$

where $\boldsymbol{D} \in \mathbb{R}^{n \times d}$ is generated by performing POD on snapshots of $\boldsymbol{b}$ from Eq. (4) (taken at the same s time steps as snapshots of $\boldsymbol{h}$) and $\boldsymbol{c} \in \mathbb{R}^{d \times 1}$ is a vector of coefficients still to be determined. Since Eq. (6) is overdetermined, only d equations are required to solve for $\boldsymbol{c}$. The retained rows of the system are the interpolation indices that are selected through the process described in Ştefănescu and Navon (2013). Defining $\boldsymbol{Z} \in \mathbb{R}^{n \times d}$ as a diminished permutation matrix that retains only the columns corresponding to the interpolation indices. Premultiplying by $\boldsymbol{Z}^T$effectively selects only the rows of $\boldsymbol{A}_h$ and $\boldsymbol{D}$ that correspond to interpolation points and Eq. (6) becomes:

$$\boldsymbol{Z}^T\boldsymbol{A}_h\ \boldsymbol{h}^{t+1} = \boldsymbol{Z}^T\boldsymbol{D}\boldsymbol{c} \tag{7}$$

Eq. (7) can be inverted to solve for $\boldsymbol{c}$ (Eq. (8)) and subsequently substituted back into Eq. (6) to obtain the final approximation of

1. Construct a basis $D \in \mathbb{R}^{n\times d}$ from POD on snapshots of a nonlinear term
2. Select z_1 as the index of the largest element of $\boldsymbol{d}_1$, the first column of D
3. For the remaining $j = 2, \ldots, d$ columns
   a. Calculate $\boldsymbol{c} = \left(Z^T\left[\boldsymbol{d}_1, \ldots, \boldsymbol{d}_j\right]\right)^{-1}\left(Z^T\boldsymbol{d}_j\right)$
      Where $Z = \left[\boldsymbol{e}_{z_1}, \ldots, \boldsymbol{e}_{z_j}\right]$
   b. Compute the residual $\boldsymbol{r} = \boldsymbol{d}_j - D\boldsymbol{c}$
   c. Take z_j to be the index of $\|\boldsymbol{r}\|_\infty$

Fig. 1. Algorithm for selecting the interpolation indices $\boldsymbol{z}_j$ for $j = 1, \ldots, d$.

the nonlinear term (Eq. (9)). Finally, POD and Galerkin projection can be applied, as in Eq. (5), to achieve a new reduced model (Eq. (10))

$$\boldsymbol{c} = \left[\boldsymbol{Z}^T\boldsymbol{D}\right)^{-1}\boldsymbol{Z}^T\boldsymbol{A}_h\ \boldsymbol{h}^{t+1} \tag{8}$$

$$\boldsymbol{A}_h\boldsymbol{h}^{t+1} \cong \boldsymbol{D}\left[\boldsymbol{Z}^T\boldsymbol{D}\right)^{-1}\boldsymbol{Z}^T\boldsymbol{A}_h\boldsymbol{h}^{t+1} \tag{9}$$

$$\boldsymbol{P}^T\boldsymbol{D}\left[\boldsymbol{Z}^T\boldsymbol{D}\right)^{-1}\boldsymbol{Z}^T\boldsymbol{A}_h\boldsymbol{P}\boldsymbol{h}_r^{t+1} = \boldsymbol{P}^T\boldsymbol{b} \tag{10}$$

All calculations dependent on the dimension n can be precomputed and the final POD-DEIM reduced model (Eq. (10)) is solved for $\boldsymbol{h}_r^{t+1}$ at each time step entirely within the reduced dimension. In other words, there are no nonlinear operations that must be carried out in the full n-dimension allowing the reduced model to be solved at each iteration depending only on dimensions r and d. Note that since $\boldsymbol{A}_h$ is a sparse matrix that results from finite difference discretization, the complexity of $\boldsymbol{A}_h\boldsymbol{P}$ scales with the dimension r, not n.

Fig. 1 shows the algorithm for selecting the interpolation indices and the steps involved in the DEIM procedure.

2.4. MODFLOW framework

The hyper-reduction within MODFLOW is performed via traditional online-offline paradigm. An additional MODFLOW package, MRED, has been created for MODFLOW-OWHM (Hanson et al., 2014) and it contains all model reduction subroutines. To further enhance the unconfined reduction capabilities, the DEIM algorithm was added to this package. The structure of the MRED package mirrors that of other MODFLOW packages. The POD-DEIM algorithm is demonstrated in the flow chart of Fig. 2. The offline portion need only be executed once for the entire simulation and the online portion is required for each iteration of the model's solver. The LAPACK LU-decomposition routine is used as the reduced solver (documented: https://software.intel.com/en-us/node/520973) and the MODFLOW implementation of the preconditioned conjugate gradient (PCG) method is used as the full model solver. When implementing solvers for reduced models, additional factors ought to be considered yet this is beyond the scope of this project; see Forstall (2015) for more thorough analysis of linear and nonlinear reduced model solvers.

2.5. Model development

First, a simple one-dimensional (1D) groundwater model was developed to test the proposed methodology. 200 finite difference cells, with a discretization of $\Delta x = 10$ m, compose the model domain. There are a total of 90 1-day time steps in the transient model, which is divided into three 30-day uniform pumping periods (referred to as stress periods). The well begins extracting on day 30, pumps for 30 days, and then shuts off for 30 days. Constant-head boundaries are set to zero units of head at nodes 1 and 200 and a pumping well is placed at node 107. The initial condition is set to zero head everywhere and a saturated thickness of 50 m. Two hydraulic conductivity zones were used ($K_{x1} = 0.4$ and $K_{x2} = 1.9$ m/day) to introduce minimal heterogeneity. The pumping rate was varied to account for uncertain pumping. The reduced model was generated with 180 snapshots: 90 snapshots with $Q = 100\ \mathrm{m}^3$/day and 90 snapshots with $Q = 200\ \mathrm{m}^3$/day. Fig. 3 displays the one-dimensional model domain with two zones and the water table contour after 30 days of pumping (i.e. at day 60) for pumping rates of 100 and 200 m^3/day. The reduced model was then tested with $Q = 150\ \mathrm{m}^3$/day to evaluate its effectiveness at pumping values not used to generate snapshots.

After the 1D case has been successfully verified, we then extend the methodology to a more realistic 2D case. The square model domain has sides of length 24,750 m and a discretization of 198 rows and 198 columns, resulting in a model grid with 39,204 uniform square cells (125 m by 125 m). The 395-day simulation has 14 stress periods: an initial 5-day period with zero pumping; 12 30-day periods with variable extractions; and a final 30-day period with zero pumping to simulate the aquifer recovery. The 5-day period has 19 time steps while other stress periods each have 13 time steps for a total of 188 time steps per simulation. The head starts at −5.0 m everywhere, creating unconfined conditions in the single layer with a thickness of 100 m. Constant head boundaries compose the top and bottom (via CHD package) while general head (GHB package) and no-flow boundaries compose the left and right boundaries. Two additional head-dependent boundary conditions—a river and a drain—were added with the RIV and DRN packages, respectively. Pumping at five production wells begins to drawdown the water table after five days. Six zones of hydraulic conductivity, all assumed to be isotropic, span four orders of magnitude. The model domain is shown in Fig. 4 with its zonation pattern and well locations. Parameter values and pumping rates for the tested model are shown in Table 2.

2.6. Snapshot selection

To mitigate for the reduced model's dependence on snapshot selection, the snapshots were taken at each time step of a simulation. Overall six simulations were used to develop the 2D snapshot set: one with all pumping rates at their respective maximums (see Table 2) and one for each of the five wells pumping at quarterly (three month) rates while all other wells are shut off. Quarterly rates for each well are 50, 75, 100, and 75% of the maximum rate for quarter 1, 2, 3, and 4, respectively. The total snapshot count is then 1128, making the snapshot sets ($\boldsymbol{\Phi}_h$ and $\boldsymbol{\Phi}_b$) matrices with dimension 39,204 × 1128. Truncated SVD on this matrix with $\varepsilon_{\text{energy}} = 99.999\%$ produces the projection matrix $\boldsymbol{P}$ and the same

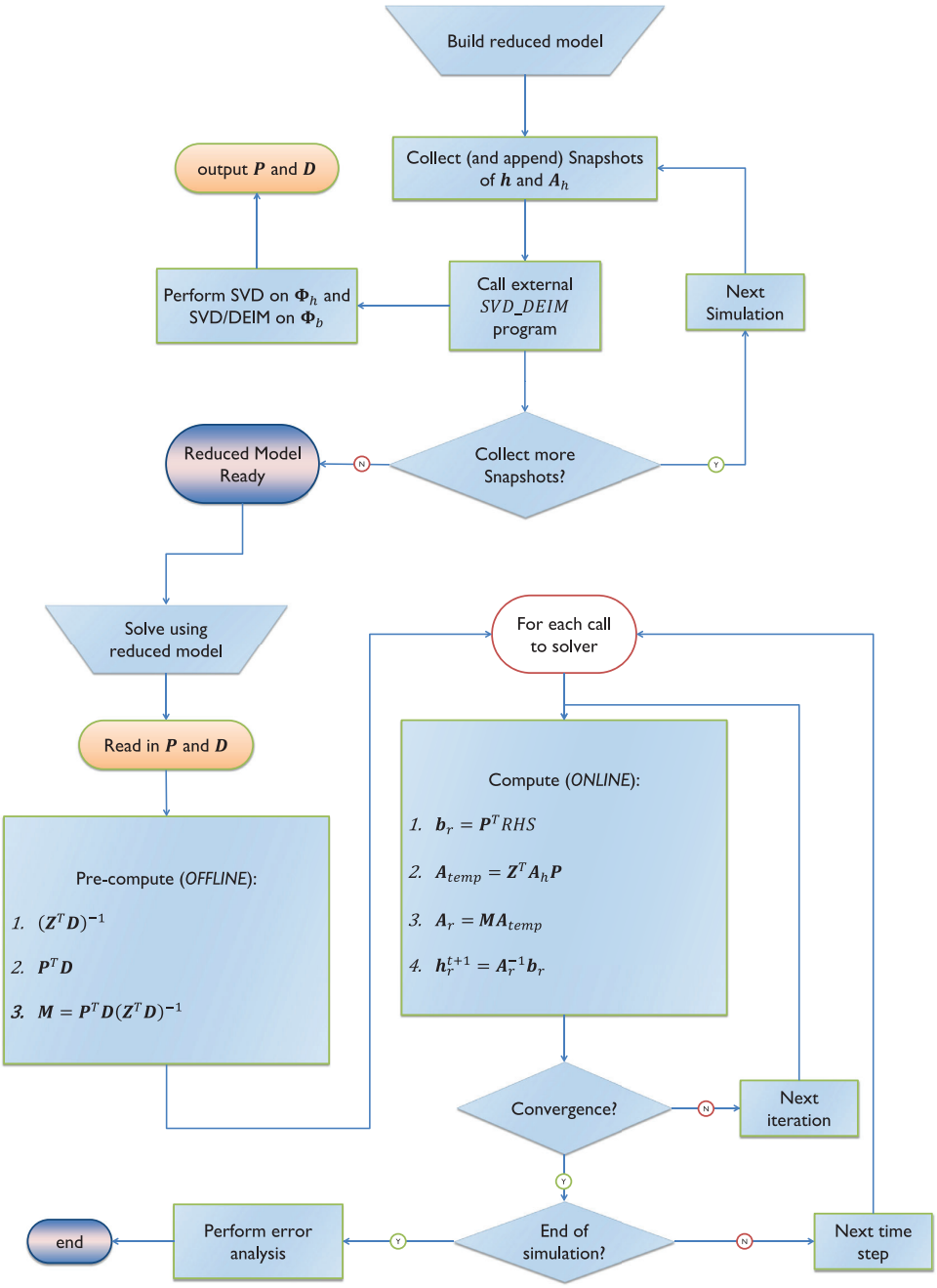

Fig. 2. The flow chart describes the process of collecting snapshots for both traditional POD and DEIM; constructing the snapshot sets and obtaining the bases; and solving with the POD-DEIM reduced model.

Table 2
Parameter and pumping values for the 2D test case.

Parameter	Value [m/day]	Pumping well	Location [row, col]	Max extraction [m^3/day]	Quarterly rates [1000 m^3/day]			
K_{x1}	0.08	1	(63, 31)	10,000	5	7.5	10	7.5
K_{x2}	5.60	2	(147, 63)	16,000	8	12	16	12
K_{x3}	8.20	3	(135, 165)	28,000	14	21	28	21
K_{x4}	10.00	4	(78, 103)	18,000	9	13.5	18	13.5
K_{x5}	18.10	5	(141, 92)	24,000	12	18	24	18
K_{x6}	22.80							

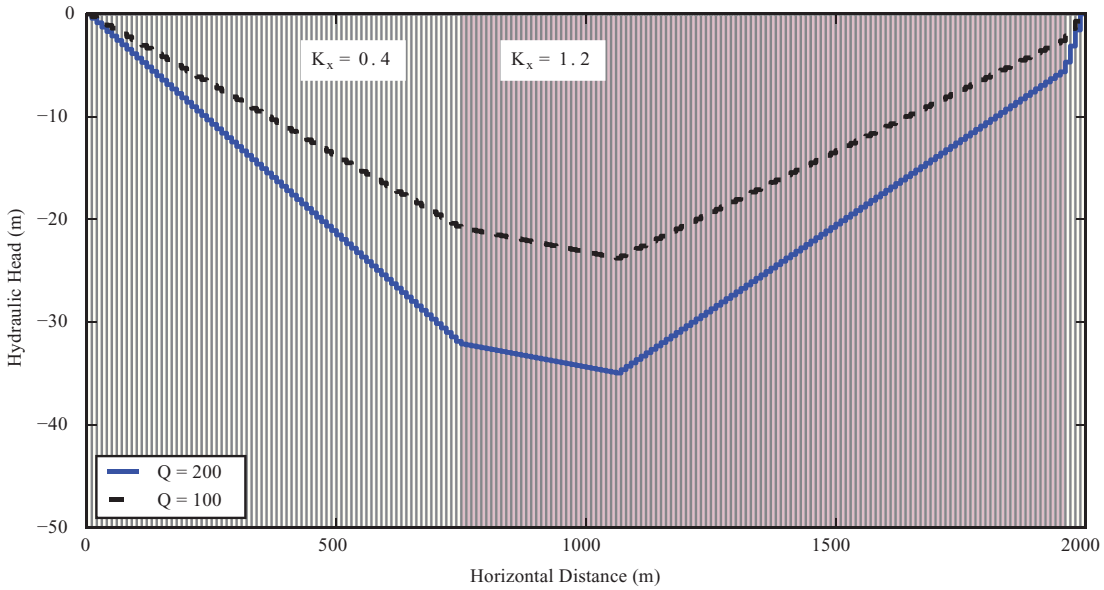

Fig. 3. The 1-dimensional model shows the conductivity zones and the water table after 30 days of pumping, creating the unconfined conditions, for pumping rates of 100 and 200 m^3/day.

method on Φ_b produces $\boldsymbol{D}$ to which DEIM is applied to obtain $\boldsymbol{Z}$. Once built, the reduced model is first tested with pumping rates at 62.5% of the maximum. Then, 50 random samples were generated to allow the pumping rates to vary between 0 and 100% for each pumping quarter.

2.7. Error analysis

The error for any reduced model is henceforth defined as the difference between the original full-model solution and the reduced model solution. This error is calculate for both the final head solution in the full model dimension as well as the nonlinear result of the operation $\boldsymbol{A}_h\boldsymbol{h}$, which is the same as the vector $\boldsymbol{b}$ for the governing equation under consideration. Absolute error is presented in meters of hydraulic head. Since, the significance of the absolute error depends on the precision of the model, the location of the maximum error is also shown in terms of the model cell number where it occurs. This information allows for quick identification of model features that may not be sufficiently captured with the current set of snapshots or interpolation points. It is not necessary for the reduced dimensions, r and d, to be the same for the POD and POD-DEIM models, they are chosen experimentally based on what is required for acceptable error. For the purposes of this paper, errors less than 1 cm are deemed insignificant. Root mean squared errors (RMSE), and normalized root mean squared error (NRMSE) are calculated for each case so the errors can be weighted by the span of head values (Eq. (11))

$$NRMSE = \frac{\| full - reduced \|_2}{\sqrt{n} * (h_{max} - h_{min})} = \frac{RMSE}{(h_{max} - h_{min})}. \quad (11)$$

3. Results

The full model (Eq. (4)) is compared to both the POD (Eq. (5)) and the POD-DEIM model (Eq. (10)) to investigate errors in the 1D test case. The absolute residual errors ($|\boldsymbol{h} - \boldsymbol{h}_r|$) between the simulated head of the full model and the POD-DEIM model are illustrated with the simulation time on the y-axis (Fig. 5). The beginning of each stress period (day 30 and day 60) can be seen to have a sharp increase in error. The maximum errors occur in the first time steps of a new stress period near the interface between the two hydraulic conductivity zones. However, the maximum error of 0.566 cm is less than 0.03% of the minimum simulated head value of −26.23 m and can be deemed insignificant. The errors diminish as the stress periods progress and the head values stabilize to a smooth gradient. A cross-section of head is also shown for the two time steps with the largest error. The reduced model head profile is indistinguishable from the full model head. Fig. 5 also shows that the full model's head distribution at the end of the first pumping period and at the beginning of the recovery period is well matched by the reduced model.

The performance of the nonlinear reduction is analyzed by comparing the result of the nonlinear operation. Fig. 6 shows the residual error ($|\boldsymbol{b} - \boldsymbol{b}_r|$) between $\boldsymbol{A}_h\boldsymbol{h}$ for the full and POD-DEIM reduced models. While minor errors still occur near the onset of a new stress period, the maximum errors now appear only at the pumping cell and persist through the entire model horizon. Distance is shown on the x-axis and time on the y-axis with shading to represent residual error. Some space and time results are omitted to focus on the only noticeable errors. Again, the errors are small with respect to the values being compared. Fig. 6 also shows a time series of head at the well and a time series of nonlinear error at the well. A very slight increase in error is observed in the aquifer recovery period over the pumping period.

Two to three orders of dimension reduction is achieved with both the 1D and 2D test problems. This reduction is quite significant, particularly for a highly discretized model. In Table 3, a summary of the reduced model's performance is compared to the full model using several metrics. The minimum head value, which is also corresponds to the maximum drawdown, is recorded to show the head range magnitude that is used to normalize the RMSE. The maximum error, maximum error location, and NRMSE are presented for both the head results and the values of the nonlinear operation $\boldsymbol{A}_h\boldsymbol{h}$. The location of the maximum error informs of the time step and cell location that would be the next choice for an added snapshot or interpolation index, respectively. The DEIM algorithm selected 5 interpolation indices for the 1D model with

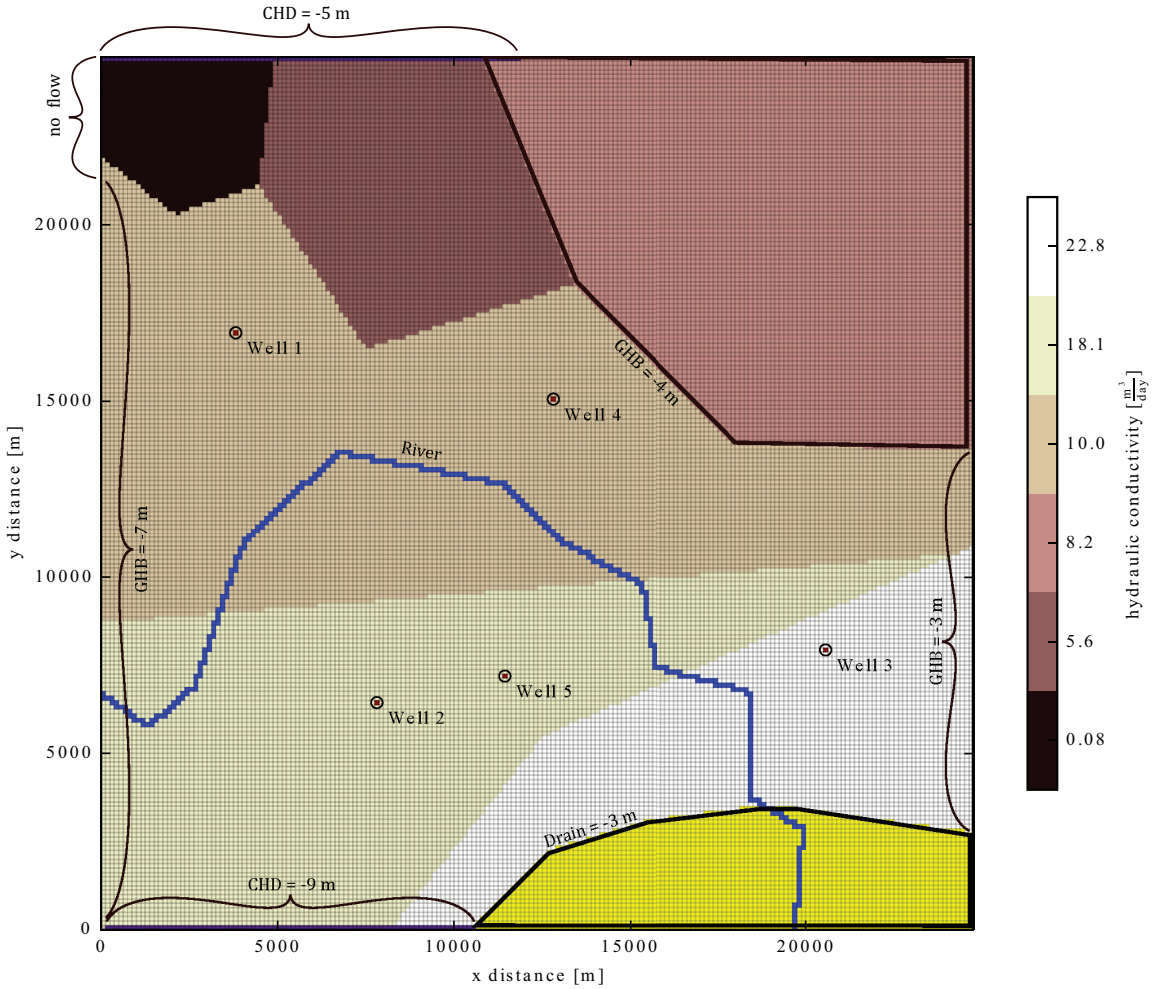

Fig. 4. The domain of the 2D test case is shown with a model grid of 198 rows and 198 columns and six conductivity zones that span several orders of magnitude. There are five wells that pump at various rates and head-dependent features (river and drain) are included.

Table 3
Model reduction results are displayed in comparison to the full, unreduced model.

				h			$A_h * h$		
		Dim	h_{min} [m]	max error [m]	max loc (t, row, [col])	NRMSE [m]	max error	max loc (t, row, [col])	NRMSE
1D	Full model	200	−26.23	–	–	–	–	–	–
1D	POD	4	−26.23	5.66E−3	(61, 69)	9.70E−2	–	–	–
1D	POD-DEIM	5	−26.23	5.66E−3	(61, 69)	9.70E−2	0.331	(61, 106)	1.64E−2
2D	Full model	39,204	−13.95	–	–	–	–	–	–
2D	POD	65	−13.95	9.3E−4	(188, 143, 153)	5.6E−6	–	–	–
2D	POD-DEIM	200	−13.95	3.2E−3	(188, 62, 90)	4.4E−5	62.9	(163, 93, 117)	1.1E−6
2D	POD-DEIM	250	−13.95	5.6E−3	(178, 30, 12)	7.1E−5	111.4	(176, 30, 12)	1.8E−6

$\varepsilon_{energy} = 99.99\%$. For the 2D model, two sets of indices were selected experimentally: one with 200 interpolation points and one with 250. The indices indicate a diverse spread across the well's capture zone in the domain's interior. Points near wells, which capture drawdown information, are often selected. Points near the boundaries are only selected if there is difficulty in resolving head-dependent boundary conditions, such as near the GHB.

For the two-dimensional case, the RMSE is calculated for each model cell over all time steps to obtain an overall assessment of the reduced model's performance. Fig. 7 displays the error in head for two versions of the 2D model: one with 200 interpolation points ($d = 200$) and one with 250 interpolation points ($d = 250$). The maximum RMSE is less than 0.02% of the span in head values (NRMSE = 0.0002) for $d = 200$ and occurs at between Well 3 and Well 4. The RMSE for $d = 250$ is distributed differently yet still extremely low throughout the entire domain. The ripple patterns emanating from some regions are a typical oscillatory behavior of POD errors. Dots mark the interpolation points identified by the DEIM algorithm. Zones with larger regions of darker shades may indicate that additional snapshots or interpolation points are

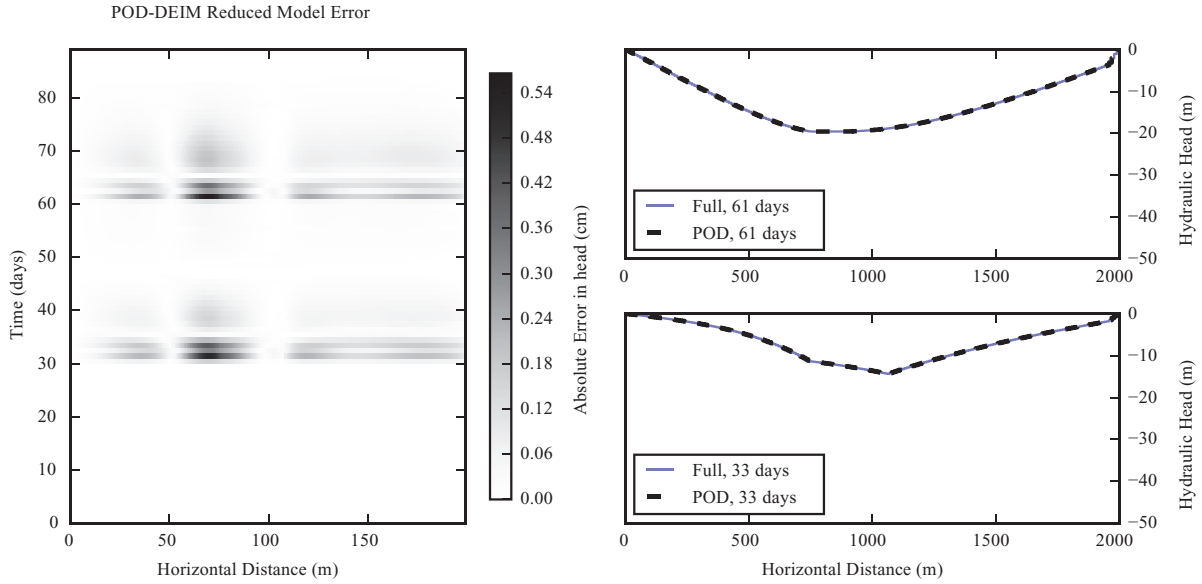

Fig. 5. (Left) The results from the 1-D test are shown as a residual between full model head and reduced model head, for each of the 90 time steps in the POD-DEIM reduced model. (Right) A cross-section of head also shows a match between the full and reduced models.

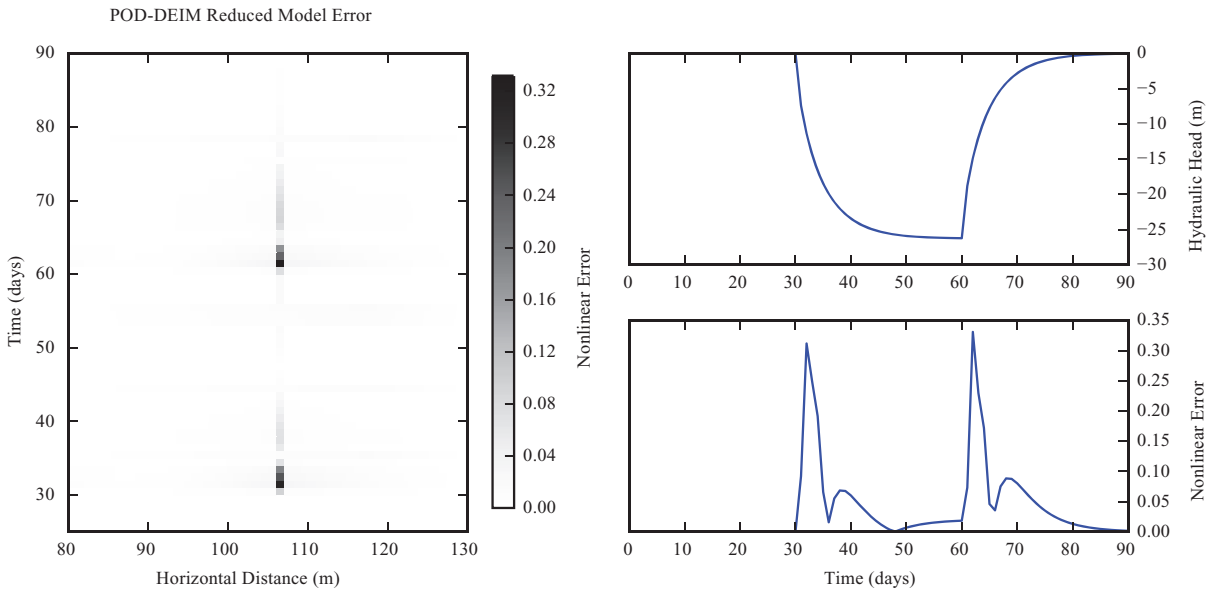

Fig. 6. (Left) The error in the nonlinear approximation is shown to be at a maximum where the well is located, cell 107, and at the beginning of each time step. (Right) A time series of head at the well is also shown above a time series of nonlinear error at the well.

needed to capture more of a response from a particular model feature.

Errors are most likely to occur where the head changes significantly from one time step to another or one model cell to another. Large head gradients are present in the vicinity of the wells and in the time step following a change in pumping rate. To test the model with these situations, Fig. 8 shows the water table plotted for two regions of the model that capture the drawdown from wells 2 and 3 (row 147 and 135, respectively). Even with significant drawdown inducing a steep head gradient toward the wells at the end of the third pumping quarter (day 305), the reduced model produces a head indistinguishable from the full model. After 395 days, the end of the simulation, the large temporal changes in head, as the water table recovers, does not produce discernable error either.

Further analysis of the error at specific time steps reveals different spatial distribution patterns. Examples of error in head and in the nonlinear term are illustrated in Fig. 9. On day 305, the largest errors in head are concentrated between Well 2 and the boundary, yet remain less than five millimeters. At 395 days, where pumping stops, the error pattern is similar, with maximum errors occurring in similar locations. A head error less than 5 mm is occurs throughout the domain. For the nonlinear error, similar spatial patterns emerge at the corresponding time steps. Even though interpolation

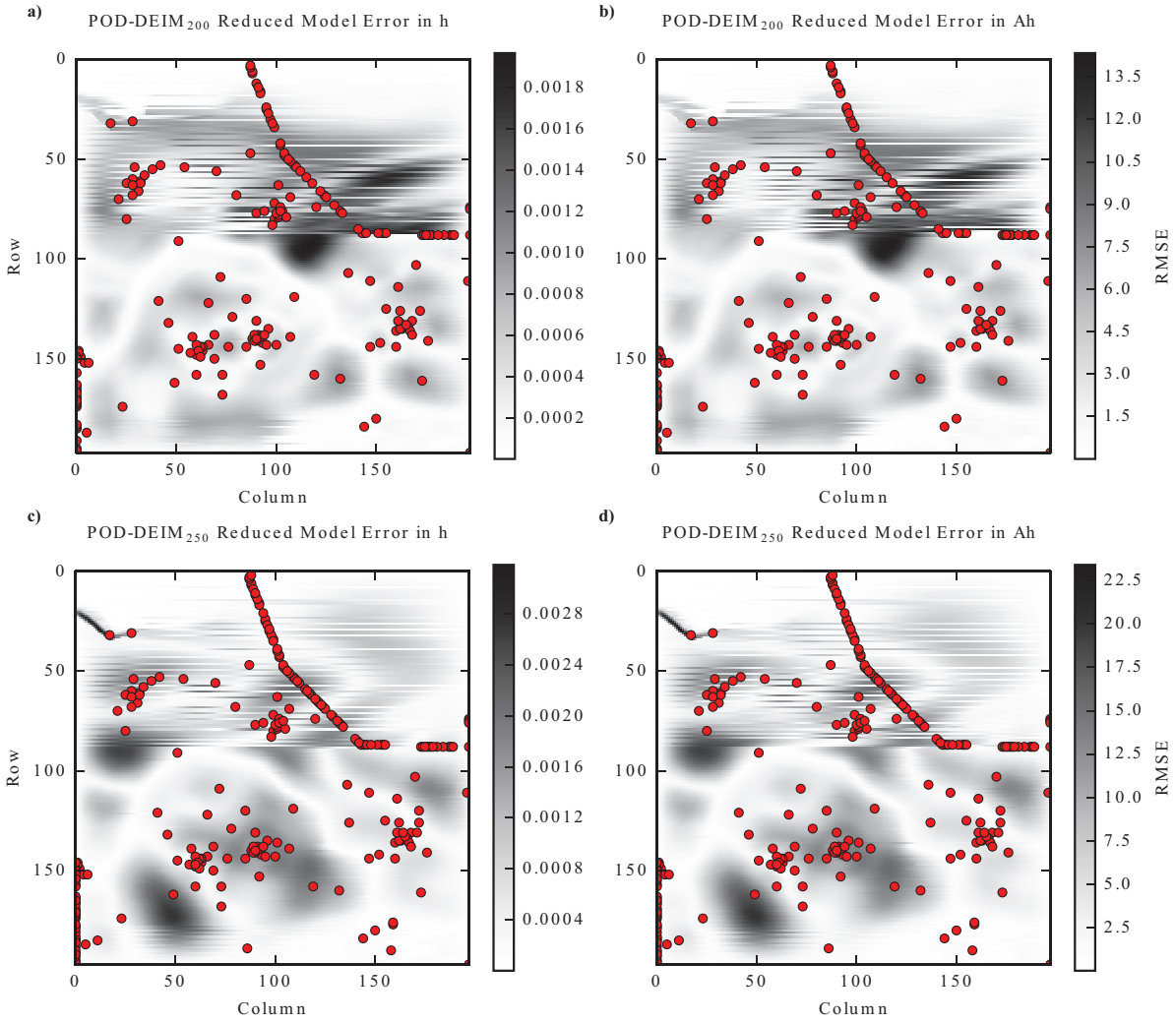

Fig. 7. The RMSE in head for each model cell is calculated over all time steps and shown over the model domain with DEIM interpolation points shown as dots. (a) Errors in **h** and (b) errors in **Ah** for the reduced model with $d=200$ are shown. Also shown are the (c) errors in **h** and (d) errors in **Ah** for the reduced model with $d=250$.

points are clustered around the wells, maximum nonlinear errors occur around the wells. The magnitude of the error in the nonlinear term has no physical interpretation but still identifies areas where the nonlinear approximation is relatively better than others. With enough interpolation points, the error pattern in the nonlinear operation closely follows that of the error in the head.

The error statistics propagate over time yet remain well below a reasonable threshold. The oscillatory error patterns are observed as small fluctuations in the time series of absolute errors shown in Fig. 10. This phenomena is commonly observed in POD-based model reduction and the propagation of error results in the largest errors occurring at the end of the simulation. The absolute error in head is shown for row 62 and column 90 (the location of the maximum error) at each time step for POD-DEIM$_{200}$ (the dual-reduced model using 200 interpolation points). The maximum absolute error spikes to 32 mm at the end of the simulation but is still within an acceptable error tolerance. For the POD-DEIM$_{250}$ model (250 interpolation points with the same dual-reduced approach), additional interpolation points level out the maximum errors at 56 mm, which now occurs at row 30 column 12. Oscillations in absolute error are attenuated as time progresses and are reduced with added interpolation points. The MAE (mean absolute error) tends to grow steadily over time but remains below 1 mm and is deemed negligible for the purposes of this study.

For a more robust test of the reduced model error, 50 model runs were performed using randomly generated pumping rates (as a fraction of the maximum). The RMSE is calculated for the head solution at each time step of each model run. Fig. 11 illustrates the exceedance curve of the RMSE for each of the reduced models. Here, another version of the reduced model, POD-DEIM$_{225}$, is also included. The POD-DEIM models are shown to reach a maximum RMSE below 1 cm a small percentage of the time and the majority of the RMSE (>60%) are below 1 mm. For the POD-DEIM$_{250}$ model, the RMSE is always less than or equal to the two other POD-DEIM versions. All RMSEs approach those of the traditional POD approach yet have superior speed.

The detailed statistical results of the 50 model runs are shown in Tables 4 and 5. Timing experiments show significant speed improvements, even for small test problems. Timing is calculated by summing the time for each call to the solver. Since both the POD

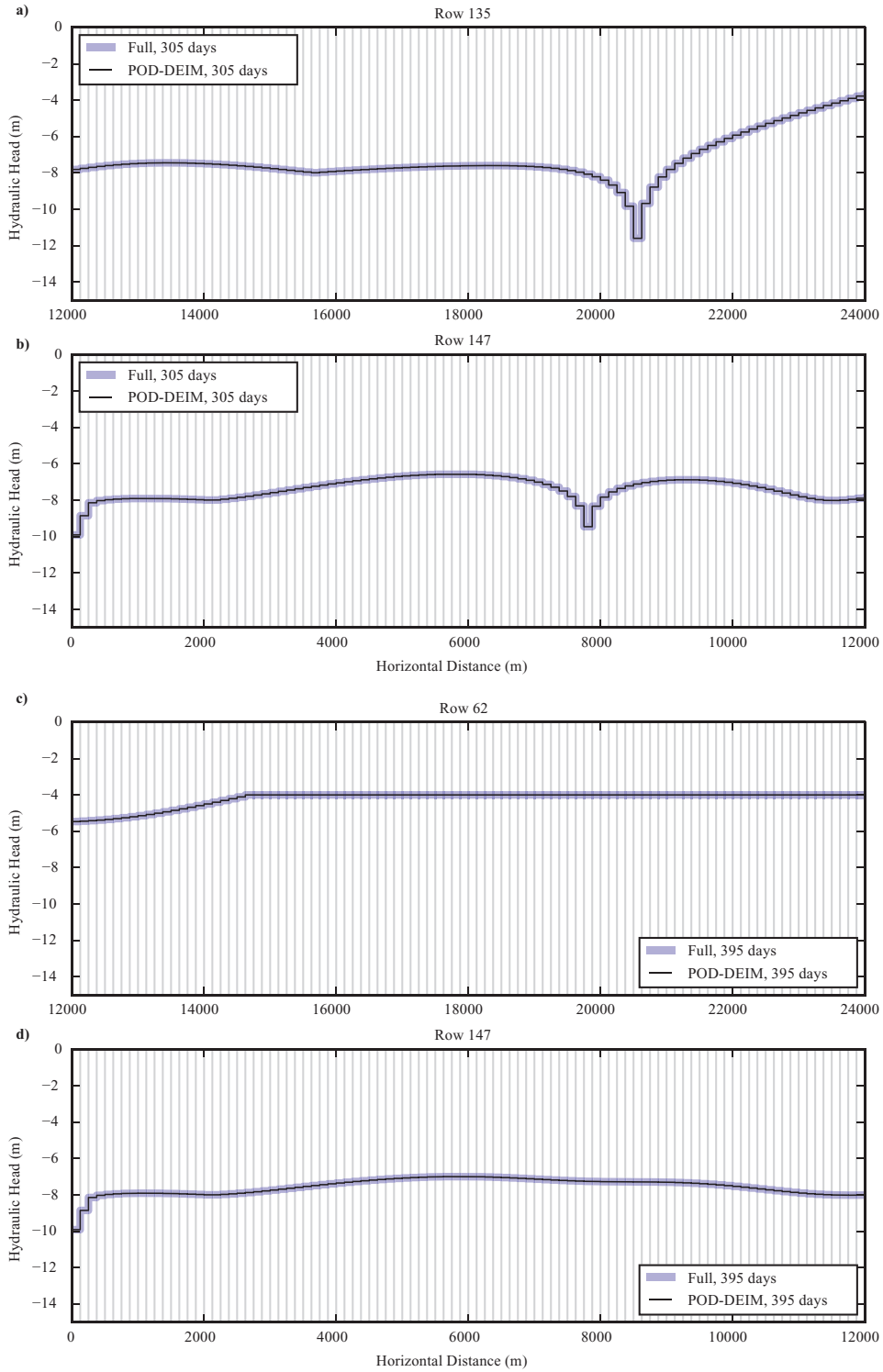

Fig. 8. The water table drawdown in selected regions is shown for the Full and POD-DEIM reduced model. Cross sections are shown for (a) 305 days at Well 3; (b) 305 days at Well 2; (c) 395 days at Well 1; and (d) 395 days at Well 2.

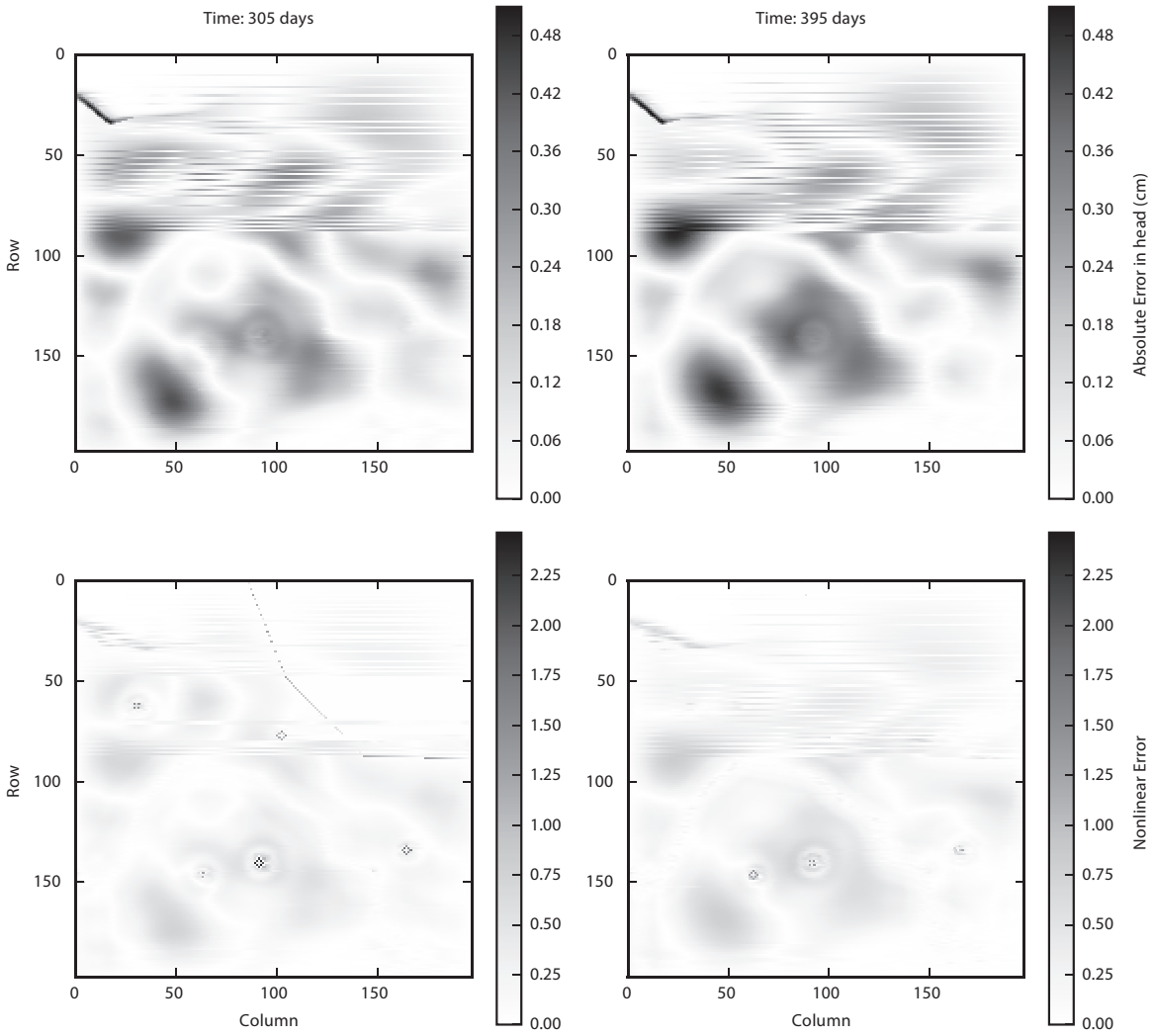

Fig. 9. (Top) The absolute error in head as well as (Bottom) the error in the nonlinear approximation are shown for (Left) day 305 and (Right) day 395, when large errors were observed.

and the POD-DEIM reduced models utilize the same solver, these times are comparable. The average speed up for the POD-DEIM$_{250}$ model over the POD model is 9.5 s while nearly equal error is obtained. Timing is not improved as additional interpolation points are added to the POD-DEIM reduced model. Though the full model utilizes a different solver, the mean total time for all calls to the PCG routine was about 3.6 s. This result indicates that for this model application, the POD reduced model causes an increase in CPU time compared to a near two-second decrease in CPU time for the POD-DEIM models. The maximum, minimum, and mean errors mostly decrease as more interpolation points are added. Similarly with the nonlinear errors, there is a unanimous decrease in errors between the POD-DEIM$_{200}$ model and the POD-DEIM$_{250}$ model.

4. Discussion

Both POD and POD-DEIM models perform well and have relatively insignificant errors. The nonlinear reduction with DEIM is obtained with only a small loss in accuracy but a gain in computational speed (Table 4). With both the 1D and 2D numerical experiments, the slight increase in approximation error is negligible when adding DEIM with an appropriate number of interpolation points. Thus, performing the nonlinear operation in the reduced space is preferable. The simplicity of the examples allows for satisfactory proof-of-concept in the 1D and 2D unconfined groundwater flow applications. Obtaining even smaller error would be feasible with additional snapshots, larger reduced dimension, or with added interpolation indices. More importantly, the dimension of the POD-DEIM$_{250}$ model reduction is from 39,204 to 250. Consequently, with POD alone, matrix calculations with a dimension on the order of 10^4 still must be performed at each iteration of the solver. The highest dimension of any matrix calculation with the POD-DEIM approach is on the order of 10^2.

More than the magnitude of the errors, the structure and distribution of the error are of interest. The results presented analyze times and zones of maximum error, which frequently occur at the beginning of stress periods. However, it is not common to require simulations to be accurate in the first few time steps of a stress period. Since it takes a few iterations for the solution to smoothly

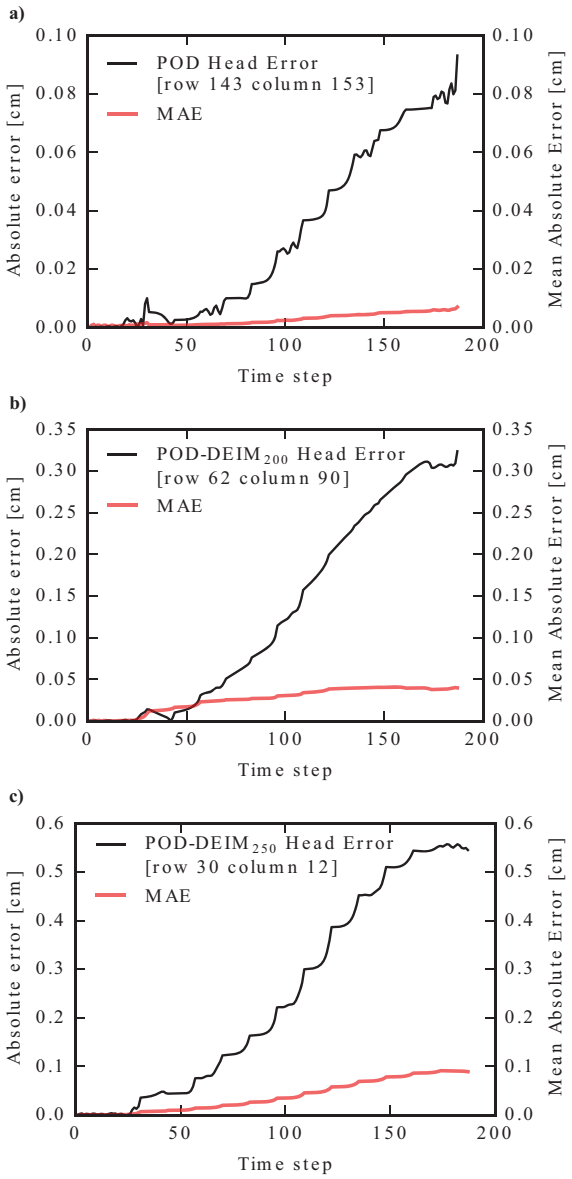

Fig. 10. Absolute error at the location found to have the largest error for the (a) POD, (b) POD-DEIM$_{200}$, and (c) POD-DEIM$_{250}$ reduced models. The MAE for the entire domain is computed for each time step and shown as a time series.

adjust heads when new forcings are introduced, it is toward the end of a stress period where results are trusted most, even in the full model. This fact allows further confidence in the reduced model's adequacy. Structurally, the oscillatory appearance of very minor errors appears as ripples in Figs. 7 and 9 and as oscillations in Fig. 10. This effect may be produced by the nature of the basis functions generated from POD and the Galerkin projection. If the errors approach levels that prohibit the application of the reduced model, alternative methods may be necessary. With careful error assessment, a new reduced model could be constructed to enhance accuracy at specific points in space and time. The error introduced from the POD-DEIM reduction is quantifiable and controllable, giving the modeler choices according to the tradeoff between reduced model

Table 4
Hydraulic head error statistics over 50 random samples for each of the 2D reduced models.

Model type	Minimum head			
	Min.	Max.	Mean	Std. dev.
POD	−18.6081	−11.3691	−14.9834	1.5532
POD-DEIM$_{200}$	−18.6083	−11.3680	−14.9838	1.5532
POD-DEIM$_{225}$	−18.6117	−11.3684	−14.9847	1.5536
POD-DEIM$_{250}$	−18.6080	−11.3693	−14.9847	1.5525
	Maximum absolute error			
	Min.	Max.	Mean	Std. dev.
POD	2.00E−03	7.48E−03	3.82E−03	1.45E−03
POD-DEIM$_{200}$	4.37E−03	1.76E−02	8.17E−03	3.25E−03
POD-DEIM$_{225}$	6.07E−03	1.76E−02	9.48E−03	2.41E−03
POD-DEIM$_{250}$	4.32E−03	1.22E−02	7.27E−03	1.82E−03
	Overall time-averaged RMSE			
	Min.	Max.	Mean	Std. dev.
POD	7.42E−05	1.89E−04	1.41E−04	2.41E−05
POD-DEIM$_{200}$	4.90E−04	1.93E−03	1.00E−03	2.89E−04
POD-DEIM$_{225}$	6.79E−04	1.46E−03	9.93E−04	1.68E−04
POD-DEIM$_{250}$	5.05E−04	1.14E−03	7.78E−04	1.33E−04
	NRMSE			
	Min.	Max.	Mean	Std. dev.
POD	2.23E−02	6.70E−02	4.02E−02	1.09E−02
POD-DEIM$_{200}$	3.86E−05	1.60E−04	8.50E−05	2.70E−05
POD-DEIM$_{225}$	5.15E−05	1.35E−04	8.45E−05	1.90E−05
POD-DEIM$_{250}$	3.50E−05	9.85E−05	6.64E−05	1.56E−05
	Time in solver			
	Min.	Max.	Mean	Std. dev.
POD	1.02E+01	1.23E+01	1.12E+01	3.83E−01
POD-DEIM$_{200}$	1.49E+00	2.49E+00	1.70E+00	1.28E−01
POD-DEIM$_{225}$	1.54E+00	1.76E+00	1.64E+00	5.43E−02
POD-DEIM$_{250}$	1.53E+00	1.82E+00	1.66E+00	5.91E−02

size, time to construct, and relative importance of some model results (time and location of head observations, for instance) more than others.

Additional strategies could be implemented to construct a more robust reduced model using the POD-DEIM method. The DEIM indices that were selected by the algorithm were unique for each specified reduced dimension. Though the specific DEIM indices were not modified, using prior knowledge of the system could allow specification of desired indices. Changes to the mesh refinement, snapshot selection, and temporal discretization could also contribute to a more accurate reduced model. Optimizing these variables is outside the scope of this study, though it is prudent to consider the amount of flexibility one would have when constructing a reduced model for more complex projects. If parameter uncertainty is a concern, systematic variation of any parameters when collecting snapshots can generate a parameter-independent reduced model (Boyce and Yeh, 2014).

For models with additional nonlinear processes, this POD-DEIM approach can be used. For more complex unconfined flow modeling in MODFLOW, these additional nonlinearities might come from more head-dependent boundary conditions (MNW, RCH, GHB, DRN, RIV) or more drawdown with additional wells. As more of these features are modeled, the simulation requires more nonlinear computations at each time step and reducing the dimension of the nonlinear term has increased benefit. If the model needs to be called 50,000 or 100,000 times—such is the case with many global heuristic search algorithms, such as a genetic algorithm—savings of

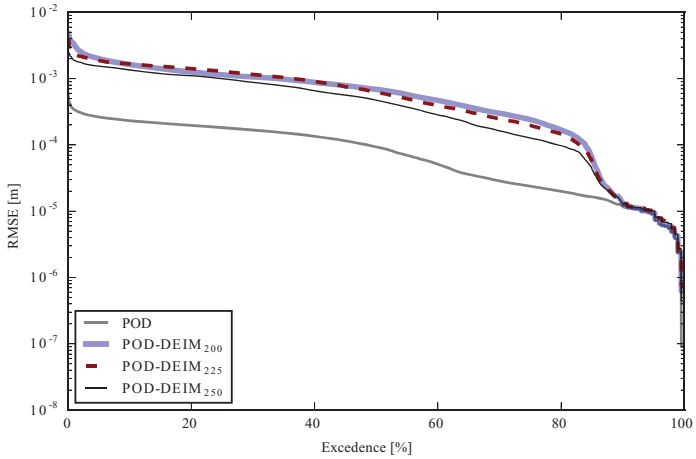

Fig. 11. A comparison of the RMSE for the residual error in head ($|\mathbf{h}-\mathbf{h}_r|$) for each of the reduced models, POD, POD-DEIM$_{200}$, POD-DEIM$_{225}$, and POD-DEIM$_{250}$ when measured against the full model.

Table 5
Nonlinear error statistics over 50 random samples for each of the 2D reduced models.

Model type	Maximum absolute error			
	Min.	Max.	Mean	Std. dev.
POD-DEIM$_{200}$	8.08E+01	3.07E+02	1.48E+02	5.32E+01
POD-DEIM$_{225}$	1.17E+02	2.92E+02	1.77E+02	4.14E+01
POD-DEIM$_{250}$	8.42E+01	2.37E+02	1.36E+02	3.16E+01
	Average RMSE			
	Min.	Max.	Mean	Std. dev.
POD-DEIM$_{200}$	3.59E+00	1.38E+01	7.26E+00	2.02E+00
POD-DEIM$_{225}$	4.92E+00	1.03E+01	7.23E+00	1.22E+00
POD-DEIM$_{250}$	3.74E+00	8.30E+00	5.70E+00	9.74E−01
	NRMSE			
	Min.	Max.	Mean	Std. dev.
POD-DEIM$_{200}$	1.11E−06	4.27E−06	2.24E−06	6.24E−07
POD-DEIM$_{225}$	1.52E−06	3.17E−06	2.23E−06	3.76E−07
POD-DEIM$_{250}$	1.15E−06	2.56E−06	1.76E−06	3.00E−07

just a few seconds in one model run can translate to a total time savings on the order of hours or days.

Hyper-reduction with POD-DEIM is an improvement over POD when it comes to versatility, efficiency and robustness. A wider range of groundwater flow processes can now be modelled in a reduced space with POD-DEIM. With only one POD projection, errors might grow too large when propagated over a long time horizon of a complex nonlinear model. To build a robust reduced model with traditional POD alone, a very large set of snapshots might be necessary to adequately approximate the nonlinear system. This often leads to only moderate dimension reduction and can increase computational cost as shown in Table 4. If reduced models are going to be used in practice, certainly online run times must be shorter than the full model. However, to decrease the overall online runtime of a full model, the online plus the offline computational cost of a reduced or hyper-reduced model ought to be considered. When snapshot selection and reduced basis construction become challenging for large-scale models, the overhead investment in the reduced model could be substantial. Therefore, POD-DEIM method allows the dimension of the online calculations to be as small as possible while still maintaining acceptable error.

Timing comparisons illustrate the practical result of dimension reduction within the context of this specific synthetic experiment. It is the reduction in dimension that has more implications for other applications. The POD-DEIM model takes about half as much time within the solver as the full model. The specific result may seem insignificant on this relatively small 2D application but when systems approach millions of nodes and decadal time horizons, any speed and dimensionality improvement will be highly beneficial. The time comparison between the full and reduced model is not entirely meaningful since different solvers are used. The PCG used for the full model is optimized for the type of problem it sees whereas the reduced model solver is more generic. Regardless of this fact, the time comparison between the reduced models is valid since they utilize the same solver. If a more efficient solver were to be used by the reduced models, the smaller dimensional complexity of the POD-DEIM model will almost always be faster to solve than the POD model.

Contrary to what one might expect, fewer interpolation points does not always lead to a faster reduced model, even though the computational complexity is less. An insufficient number of interpolation points induces more error and requires more internal solver iterations for convergence. In practice, keeping the volumetric water budget percent error below a nominal value set by MODFLOW has been a good indication of a robust interpolation.

While construction of the POD-DEIM reduced model can still be time intensive, the possible applications to a variety of problems can exploit the superior speed. For example, multi-objective optimizations or large computer experiments involving Monte Carlo can require thousands or millions of model calls. For many developed groundwater models, run times for a single simulation can approach days. Consequently, some types of optimizations or uncertainty analyses would be infeasible without model reduction. Any opportunity to reduce the dimensionality of model's calculations may permit what was previously infeasible. The methodology proposed could specifically be used within parameter estimation techniques used to estimate unknown pumping rates to match drawdown observations—a problem encountered during a calibration process when wells that lack pumping data are modeled within a groundwater basin. It may also be necessary to quantify the uncertainty of the pumping rate estimates to supplement any model predictions. If the proposed POD-DEIM methodology is used within an uncertainty analysis—such as the null-space Monte Carlo used by Siade et al. (2015)—further time savings could be

achieved. For more versatile applications to parameter estimation, the following steps can be taken: (1) take snapshots to capture a range of any parameter; (2) add them to the snapshot set; and (3) re-compute the basis.

There are some aspects that still need to be explored with POD-DEIM models as the size of the application scales up. For models that would not permit taking snapshots at every time step, methods for optimal snapshot selection ought to be considered. The choice of snapshots could be the difference between a reduced model that converges in the solver and one that does not. In cases where groundwater flow models are coupled to transport, rainfall-runoff, and/or atmospheric models, the reduced model's solution serves as input to these other models. The oscillatory nature of the reduced model's errors would have an unknown effect on models to which it may be coupled. Further research could also explore the trade-off in the size of dimensions r and d; the appropriateness of the percent energy criteria used to select the reduced dimensions; and applications of more efficient solvers for the reduced models.

5. Conclusion

A traditional model reduction technique for groundwater flow has been combined with an interpolation scheme to further reduce nonlinear components. The result is a reduced model of an unconfined flow equation that can be solved entirely in the reduced dimension with no dependence on the original, full model complexity. This additional approximation allows for faster calculations of nonlinear operations at each time step while sacrificing a tractably small amount of accuracy. As simulation models get more complex, with finer discretization, larger domains, and more nonlinear processes, faster calculations become more important. The combined model reduction approach with POD and DEIM greatly improves a modeler's ability to obtain solutions quickly. The results from the two test problems show a two to three orders of dimension reduction. A key advantage of the POD-DEIM model is that nonlinear operations are carried in the reduced space. The faster overall simulation times are critical when embedding within or linking the model to any form of optimization (e.g., parameter estimation, experimental design, resource allocation) or extensive uncertainty analysis (e.g., Monte Carlo). While more and more optimization algorithms are taking advantage of parallel computing power, long simulation runtimes still inhibit the attainment of optimal solutions in reasonable amounts of time. Therefore, reduced models such as those developed with POD-DEIM can be used within parallel architectures to facilitate searching very large feasible regions—regions with dimensions so large that they would otherwise be impossible to explore.

Acknowledgments

This material is based on work supported by NSF under Award EAR-1314422. Partial support also was provided by an AECOM endowment. The in-depth reviews and constructive comments provided by two anonymous reviewers are greatly appreciated.

References

Abgrall, R., Amsallem, D., 2016. Robust model reduction by L1-norm minimization and approximation via dictionaries: application to linear and nonlinear hyperbolic problems. Adv. Model. and Simul. in Eng. Sci. 3 (1), 1–6. http://dx.doi.org/10.1186/s40323-015-0055-3.

Antoulas, A., Sorensen, D., Gugercin, S., 2001. A survey of model reduction methods for large-scale systems. Contemp. Math. 280, 193–220. http://dx.doi.org/10.1080/00207170410001713448.

Barrault, M., Maday, Y., Nguyen, N.C., Patera, A.T., 2004. An "empirical interpolation" method: application to efficient reduced-basis discretization of partial differential equations. C. R. Math. 339, 667–672. http://dx.doi.org/10.1016/j.crma.2004.08.006.

Boyce, S.E., Nishikawa, T., Yeh, W.W.-G., 2015. Reduced order modeling of the Newton formulation of MODFLOW to solve unconfined groundwater flow. Adv. Water Resour. 83, 250–262. http://dx.doi.org/10.1016/j.advwatres.2015.06.005.

Boyce, S.E., Yeh, W.W.-G., 2014. Parameter-independent model reduction of transient groundwater flow models: application to inverse problems. Adv. Water Resour. 69, 168–180. http://dx.doi.org/10.1016/j.advwatres.2014.04.009.

Cardoso, M.A., Durlofsky, L.J., Sarma, P., 2009. Development and application of reduced-order modeling procedures for subsurface flow simulation. Int .J. Numer. Methods Eng. 77, 1322–1350. http://dx.doi.org/10.1002/nme.2453.

Chaturantabut, S., Sorensen, D.C., 2010. Nonlinear model reduction via discrete empirical interpolation. SIAM J. Sci. Comput. 32, 2737–2764.

Drohmann, M., Haasdonk, B., Ohlberger, M., 2012. Reduced basis approximation for nonlinear parametrized evolution equations based on empirical operator interpolation. SIAM J. Sci. Comput. 34, A937–A969. http://dx.doi.org/10.1137/10081157x.

Forstall, V.H., 2015. Iterative solution methods for reduced-order models of parameterized partial differential equations, Doctoral dissertation. University of Maryland, College Park.

Graham, M., Kevrekidis, I., 1996. Alternative approaches to the Karhunen–Loeve decomposition for model reduction and data analysis. Comput. Chem. Eng. 20, 495–506. http://dx.doi.org/10.1016/0098-1354(95)00040-2.

Hanson R.T., Boyce S.E., Schmidt W., Hughes J.D., Mehl S.M., Leake S.A., et al., 2014. One-water hydrologic flow model (MODFLOW-OWHM), U.S. Geological Survey Techniques and Methods 6–A51, 120 p., http://dx.doi.org/10.3133/tm6A51.

Henneron, T., Clenet, S., 2014. Model order reduction of non-linear magnetostatic problems based on POD and DEI methods. IEEE Trans. Magn. 50, 33–36. http://dx.doi.org/10.1109/TMAG.2013.2283141.

Hill, M.C., 1990. Preconditioned conjugate-gradient 2 (PCG2), a computer program for solving ground-water flow equations. Water-Resources Investigations Report. US Geological Survey, p. 43.

Kasprzyk, J.R., Reed, P.M., Kirsch, B.R., Characklis, G.W., 2009. Managing population and drought risks using many-objective water portfolio planning under uncertainty. Water Resour Res 45 (12), W12401. http://dx.doi.org/10.1029/2009WR008121.

Keating, E., Zyvoloski, G., 2009. A stable and efficient numerical algorithm for unconfined aquifer analysis. Ground Water 47, 569–579. http://dx.doi.org/10.1111/j.1745-6584.2009.00555.x.

McPhee, J., Yeh, W.W.-G, 2008. Groundwater management using model reduction via empirical orthogonal functions. J. Water Resour. Plan. Manag. 134, 161–170. http://dx.doi.org/10.1061/(ASCE)0733-9496(2008)134:2(161).

Nigro, P.S.B., Anndif, M., Teixeira, Y., Pimenta, P.M., Wriggers, P., 2015. An adaptive model order reduction with quasi-Newton method for nonlinear dynamical problems. Int. J. Numer. Methods Eng. 106 (9), 740–759. http://dx.doi.org/10.1002/nme.5145.

Niswonger, R.G., Panday, S., Ibaraki, M., 2011. MODFLOW-NWT, a Newton formulation for MODFLOW-2005. US Geological Survey Techniques and Methods 6-A37. US Geological Survey, p. 44.

Quarteroni, A., Rozza, G., 2007. Numerical solution of parametrized Navier–Stokes equations by reduced basis methods. Numer. Methods Partial Differ. Equ. 23, 923–948. http://dx.doi.org/10.1002/num.20249.

Radermacher, A., Reese, S., 2015. POD-based model reduction with empirical interpolation applied to nonlinear elasticity. Int. J. Numer. Methods Eng. 107 (6), 477–495. http://dx.doi.org/10.1002/nme.5177.

Reed, P.M., Hadka, D., Herman, J.D., Kasprzyk, J.R., Kollat, J.B., 2013. Evolutionary multiobjective optimization in water resources: the past, present, and future. Adv. Water Resour. 51, 438–456. http://dx.doi.org/10.1016/j.advwatres.2012.01.005.

Reyment, R.A., Joreskog, K.G., 1993. Applied Factor Analysis in the Natural Sciences. Cambridge University Press.

Siade, A., Nishikawa, T., Martin, P., 2015. Natural recharge estimation and uncertainty analysis of an adjudicated groundwater basin using a regional-scale flow and subsidence model (Antelope Valley, California, USA). Hydrogeol. J. 23, 1267–1291. http://dx.doi.org/10.1007/s10040-015-1281-y.

Siade, A.J., Putti, M., Yeh, W.W.-G., 2012. Reduced order parameter estimation using quasilinearization and quadratic programming. Water Resour. Res. 48 (6), W06502. http://dx.doi.org/10.1029/2011WR011471.

Sirovich, L., 1987. Turbulence and the dynamics of coherent structures. Part I: coherent structures. Q. Appl. Math. 45 (3), 561–571.

Ştefănescu, R., Navon, I.M., 2013. POD/DEIM nonlinear model order reduction of an ADI implicit shallow water equations model. J. Comput. Phys. 237, 95–114. http://dx.doi.org/10.1016/j.jcp.2012.11.035.

Ştefănescu, R., Sandu, A., Navon, I.M., 2015. POD/DEIM reduced-order strategies for efficient four dimensional variational data assimilation. J. Comput. Phys. 295, 569–595. http://dx.doi.org/10.1016/j.jcp.2015.04.030.

Tonkin, M., Doherty, J., 2009. Calibration-constrained Monte Carlo analysis of highly parameterized models using subspace techniques. Water Resour. Res. 45, 1–17. http://dx.doi.org/10.1029/2007WR006678.

Vermeulen, P.T.M., Heemink, A.W., Te Stroet, C.B.M., 2004. Reduced models for linear groundwater flow models using empirical orthogonal functions. Adv. Water Resour. 27, 57–69. http://dx.doi.org/10.1016/j.advwatres.2003.09.008.

Vermeulen, P.T.M., Heemink, A.W., Te Stroet, C.B.M., 2004. Low-dimensional modelling of numerical groundwater flow. Hydrol. Process. 18, 1487–1504. http://dx.doi.org/10.1002/hyp.1424.

von Storch, H., Hannoschöck, G., 1985. Statistical aspects of estimated principal vectors (EOFs) based on small sample sizes. J. Clim. Appl. Meteorol. 24, 716–724.

Willis, R., Yeh, W.W.-G., 1987. Groundwater Systems Planning and Management. Prentice Hall Inc., Old Tappan, NJ.

3.

Advances in Water Resources 130 (2019) 157–171

Contents lists available at ScienceDirect

Advances in Water Resources

journal homepage: www.elsevier.com/locate/advwatres

Nonlinear model reduction of solute transport models

Zachary P. Stanko, William W.-G. Yeh*

Department of Civil and Environmental Engineering, University of California, Los Angeles, CA, 90095 USA

ARTICLE INFO

Keywords:
Model reduction
Solute transport
Proper orthogonal decomposition
Discrete empirical interpolation
Nonlinear differential equations

ABSTRACT

Computer simulations of groundwater flow and solute transport are often burdened by long runtimes. The simulations are necessarily complex to capture the system dynamics and finely discretized spatial and temporal domains are often needed for solution accuracy and stability. Model reduction allows for the approximation of system state by solving equations in a reduced dimensional space. Proper orthogonal decomposition (POD) is an effective way to reduce the dimensionality of systems of differential equations that are discretized by finite difference or finite element methods. If the problems are nonlinear in nature, the discrete empirical interpolation method (DEIM) has been shown to supplement POD by further reducing the dimension of nonlinear calculations. Here, the combined POD-DEIM approach is shown to work on a problem of 2-dimensional groundwater flow with solute transport exhibiting nonlinear sorption. The application is restricted to largely dispersive problems (low Peclet number). Results show areas of high concentration are effectively identified with mean errors less than 2% of the full model.

1. Introduction

Groundwater flow and solute transport models often present a high demand on computational resources. The groundwater flow component and solute transport component must be solved separately and are often coupled together. Either the flow or the transport component may be nonlinear if representing unconfined conditions or nonlinear sorption/reaction, respectively. Nonlinear problems require additional solver iterations for each time-step. The solution dimensionality of these models is determined by the number of cells in the finite difference or finite element mesh. As the modelled region becomes larger, and/or spatial discretization becomes finer, the number of cells can be in the millions. Added computational demand arises when modeling transient conditions for a long time horizon. The highest degree of complexity occurs when density-dependence is considered, and the flow and transport solutions must have yet another additional iteration between the two component solutions at each time-step. One consequence of modeling complex systems with high-fidelity models is that completing one simulation can take hours or even days. Even with a substantial number of modern CPUs, any type of problem that involves running a high-dimensional groundwater flow and solute transport model thousands of times (e.g., parameter estimation, Monte Carlo, or management optimizations) can be impractical or even infeasible. The option to use a lower fidelity model that has fewer cells and/or time steps may be appealing but is often accompanied by large reductions in accuracy. Model reduction techniques are a way to reduce the dimension of solution space at each time step, thereby reducing total runtimes of the simulation model so that many types of problems become solvable in a reasonable amount of time with acceptable reduced-model error.

While being a new field of research, model reduction for groundwater flow models has been well-studied. A popular model reduction technique for groundwater flow is to use proper orthogonal decomposition (POD) to identify a lower dimensional basis on which to project the high-dimensional model (McPhee and Yeh, 2008). Many variations of POD-based model reduction have been proposed in the literature for linear/confined groundwater flow problems (Boyce et al., 2015; Boyce and Yeh, 2014; McPhee and Yeh, 2008; Pasetto et al., 2013; Siade et al., 2012; Vermeulen et al., 2004a, 2004b). Alternatively, there are other methods of surrogate modeling, such as data-driven approaches, which also achieve the desired outcome of a reduced model but do not intrinsically represent the known physics of the system being simulated. These other methods are reviewed in Asher et al., 2015.

An additional reduced modeling technique is needed to address the problematic nature of POD-based model reduction on nonlinear problems, in which there are still calculations that scale up with the dimension of the full model. The discrete empirical interpolation method (DEIM) was introduced to formulate a reduced model with a solution complexity that scaled only with reduced dimensions (Chaturantabut and Sorensen, 2010). POD and DEIM have been combined in a shallow groundwater context to show the effectiveness of the dual-reduction approach (Ştefănescu and Navon, 2013). Recent developments have also allowed for model reduction for

* Corresponding author.
E-mail address: williamy@seas.ucla.edu (W.W.-G. Yeh).

https://doi.org/10.1016/j.advwatres.2019.05.028
Received 5 October 2018; Received in revised form 31 May 2019; Accepted 31 May 2019
Available online 5 June 2019
0309-1708/© 2019 Elsevier Ltd. All rights reserved.

nonlinear/unconfined groundwater flow by supplementing a POD-based reduced model with DEIM to approximate nonlinear calculations (Stanko et al., 2016). This recent work not only showed the effectiveness of the dual approach, but also implemented it within the commonly used software MODFLOW (Harbaugh, 2005), specifically MODFLOW-OWHM (Hanson et al., 2014). The combined approach serves to reduce the dimension of nonlinear operations while sacrificing acceptable increases in error, and with error bounds that are tractable (Chaturantabut and Sorensen, 2010).

In contrast to the concept of model reduction for groundwater flow, model reduction research for solute transport is in its very early stages. Robinson et al. (2012) has shown that similar POD-based model reduction techniques can work for linear solute transport models solving the advection-dispersion equation. In that work, a small (< 1 m^2) two-dimensional finite element model with linear sorption was reduced and solved within the Finite-Element Heat- and Mass-Transfer (FEHM) code. Research in POD reduced modeling for advection-dispersion has shown sensitivity to snapshot selection and better performance with a randomly generated realization of heterogeneous media when compared to the zonal approach (Li and Hu, 2013). Rizzo et al. (2018) further demonstrated the effectiveness of a POD-based approach to model reduction of linear solute transport models with enhancements such as an adaptive snapshot splitting technique which showed improved performance with low Peclet numbers. Additional work has demonstrated successful POD-based model reduction on a variable-density flow and transport problem (Li et al., 2013) but this work suggested the need for a modified approach, like DEIM, to address mathematical nonlinearities that cause significant errors in long-term predictions with POD-based reduced models.

Since DEIM has been effective in reducing various nonlinear models (Tezduyar et al., 2008; Chaturantabut and Sorensen, 2011; Dimitriu et al., 2014; Xiao et al., 2014), it is a likely candidate for modeling nonlinear solute transport when coupled with groundwater flow. One of the benefits of a dual model reduction approach to a coupled flow and transport model is the reduction in number of nonlinear operations, too many of which can hinder the application of such models. It is also likely that repeated calculations of solute concentration in areas of low concentration within a large groundwater flow model are not necessary. For problems involving a contaminant plume or seawater intrusion, the location of a high-concentration region within a much larger groundwater domain is desired. Model reduction via POD and DEIM may help approximate concentrations in these areas while maintaining high computational efficiency. The following section provides the derivation of POD-DEIM for an advection-dispersion equation that includes nonlinear sorption. This study then applies this method to one-dimensional (1-D) and two-dimensional (2-D) nonlinear solute transport simulations. To date, this is the only known application of POD-DEIM reduced models to nonlinear solute transport.

2. Methodology

The following methodology introduces the equations for groundwater flow and solute transport. Reduced modeling by POD and DEIM will be derived for the transport equation. The implementation of these methods within the commonly used MT3DMS software (Zheng and Wang, 1999) framework—as updated by Bedekar et al. (2016)—will be described. All variable definitions are compiled in Table 1 with the following convention: uppercase letters for scalar variables; bold lowercase for one-dimensional vectors; bold uppercase for two-dimensional matrices.

2.1. Groundwater flow

The groundwater flow equations that are employed in this method are the unadulterated versions that are described in Harbaugh (2005). MODFLOW-2005 is used to generate a steady flow field as input to the transport model. In more advance simulations, this would be an iterative process; however, to address the specific intention of nonlinear solute transport model reduction, the flow system is assumed to be steady and need only be generated once and provided to the transport simulation as a flow velocity field. For this experiment, the groundwater flow equations are not reduced as they were in Stanko et al. (2016); instead, the full flow solution is retained to isolate the solute transport reduction process.

2.2. Solute transport

Solute transport is modeled by way of the advection-dispersion-reaction equation as it is incorporated into the updated software MT3D-USGS (Bedekar et al., 2016). The newer version of MT3D provides several additional features not present in the original MT3DMS software. The new software corrects a small error that caused mass to not be conserved in some cases, facilitates solute transport calculations in additional groundwater flow packages (as well as in the unsaturated zone), and adds flexibility to the solution scheme by manipulating the way some terms are incorporated into the solution scheme. Implementing the reduced modeling approach within this code ensures its usefulness for the latest generation of simulation programs.

2.2.1. Governing equation

The following equation is a full three-dimensional representation of advection, dispersion, and reaction of a single solute in a groundwater flow system as presented in Zheng (2009) with units representing the current application:

$$\theta \frac{\partial C^k}{\partial t} = \frac{\partial}{\partial x_i}\left(\theta D_{ij} \frac{\partial C^k}{\partial x_j}\right) - \frac{\partial}{\partial x_i}\left(\theta v_i C^k\right) + q_s C_s^k - q_s' C^k + \sum R_n \tag{1}$$

where

θ = porosity of the subsurface medium, dimensionless
C^k = dissolved concentration of species k, [g/m^3]
t = time, [days]
$x_{i,j}$ = distance along the respective Cartesian coordinate axis, [m]
$D_{i,j}$ = hydrodynamic dispersion coefficient tensor, [m^2/day]
v_i = seepage or linear pore water velocity, [m/day] it is related to the specific discharge or Darcy flux through the relationship: $v_i = \frac{q_i}{\theta}$
q_s = volumetric flow rate per unit volume of aquifer representing fluid sources (positive) and sinks (negative), [1/day]
C_s^k = concentration of the source or sink flux for species k, [g/m^3]
ΣR_n = chemical reaction terms, [g/ m^3 day]

Eq. (1) is modified by expanding the time-derivative and reaction term and simplified by dropping the species index (henceforth assuming only one species of solute is present) to obtain Eq. (2) (Eq. (4), Zheng and Wang 1999).

$$\theta \frac{\partial C}{\partial t} + \rho_b \frac{\partial \bar{C}}{\partial t} = \frac{\partial}{\partial x_i}\left[\theta D_{ij} \frac{\partial C}{\partial x_j}\right] - \frac{\partial}{\partial x_i}\left(\theta v_i C\right) + q_s C_s - q_s' C - \lambda_1 \theta C - \lambda_2 \rho_b \bar{C} \tag{2}$$

Where C and $\bar{C}$ are concentrations of the dissolved and sorbed phases, respectively; q_s' is the rate of change in transient groundwater storage; $\lambda_1 \theta C$ and $\lambda_2 \rho_b \bar{C}$ are terms representing first order reaction (with reaction rates λ_1 and λ_2) for the dissolved and sorbed phases, respectively; and ρ_b is the bulk density of the porous media in g/m^3. The translation of Eq. (2) is a mass balance at any given time between dissolve/sorbed mass and the difference between mass inflow and mass outflow, controlled by advection, dispersion, reaction, and sources/sinks. It is assumed that local equilibrium exists for any sorption or reaction (Zheng and Wang, 1999). For this research the Freundlich isotherm is employed to simulate equilibrium nonlinear

Table 1
Variable symbols and definitions along with appropriate units.

Symbol	Dimension	[units]	Description
$\boldsymbol{h}$	$n\times 1$	[m]	Vector of groundwater head
$\boldsymbol{c}$	$n\times 1$	[g/m^3]	Vector of solute concentration
$\boldsymbol{A}_c$	$n\times n$	[-]	Matrix containing nonlinear coefficients for the solute transport equation (elements that are functions of concentration)
$\boldsymbol{b}$	$n\times 1$	[-]	Right-hand side vector of the groundwater flow equation
$\boldsymbol{K}_x$, $\boldsymbol{K}_y$	$n\times n$	[m/day]	Hydraulic conductivity in the x and y principal directions
$\boldsymbol{D}$	$n\times n$	[m^2/day]	Hydrodynamic dispersion coefficient tensor
α_L	scalar	[m]	Longitudinal dispersivity
α_T	scalar	[m]	Transverse dispersivity
$\boldsymbol{R}(\boldsymbol{c})$	$n\times 1$	[-]	Retardation factor (function of $\boldsymbol{c}$ for nonlinear sorption)
ρ_b	scalar	[g/m^3]	Bulk density of the subsurface material
λ_1	scalar	[1/day]	First-order reaction rate for the dissolved phase
λ_2	scalar	[1/day]	First-order reaction rate for the sorbed phase
$\boldsymbol{Q}$	$n\times 1$	[m/day]	Sources/sinks of water in flow per unit volume
q_s	scalar	[1/day]	Volumetric flow rate of source/sink per unit volume
q_c	scalar	[g/day]	Mass-loading rate of solute entering the system
v_i	scalar	[m/day]	Seepage or linear pore water velocity
S_y	scalar	[-]	Specific yield coefficient
θ	scalar	[-]	Porosity of the subsurface medium
K_f	scalar	[m^3/day][a]	Freundlich constant
a	scalar	[-]	Freundlich exponent
Pe	scalar		Peclet number
ϵ_{max}	scalar	[m]	Maximum difference in head in two consecutive iterations.
i, j	scalar		Indices for the model cells in the x and y direction
t	scalar		Index for the model time steps
n	scalar	[-]	Number of finite difference cells of the model domain
r	scalar	[-]	Number of singular values retained from POD to create the reduced model
s	scalar	[-]	Number of snapshots taken of the full model
d	scalar	[-]	Number of interpolation points used for the POD-DEIM reduced model
Δ_t	scalar	[days]	Time step length
$\boldsymbol{\Phi}_c$	$s\times n$		Snapshot set of $\boldsymbol{C}$.
$\boldsymbol{\Phi}_b$	$s\times n$		Snapshot set of b.
σ_i	scalar		The i^{th} singular value
$\mathbf{P}$	$n\times r$		Projection matrix formed from POD on Φ_h
$\mathbf{D}$	$n\times d$		Projection matrix formed from POD on Φ_d
$\mathbf{Z}$	$n\times d$		Permutation matrix to select the dominant rows of the system
z_j	scalar		The j^{th} interpolation index
$\boldsymbol{z}$	$d\times 1$		Vector of reduced variables in DEIM formulation
$\boldsymbol{c}_r$	$r\times 1$		Vector of state variables in the reduced space
$\boldsymbol{z}_m$	$d\times 1$		Vector of interpolation indices for model m.

sorption as $\bar{C} = K_f C^a$, where K_f is the Freundlich constant and a is the Freundlich exponent. Eq. (2) can be re-written as:

$$R\theta\frac{\partial C}{\partial t} = -\frac{\partial}{\partial x}\left(\theta v_x C\right) - \frac{\partial}{\partial y}\left(\theta v_y C\right) - \frac{\partial}{\partial z}\left(\theta v_z C\right) + L(C) \tag{3}$$

Where $L(C)$ represents all terms not related to advection (i.e., dispersion, sources, reactions). Derivatives in Eq. (3) are approximated in space and time by an implicit finite difference algorithm with an upstream weighting scheme. Details of the derivations are provided in Zheng and Wang (1999). The retardation factor for systems simulating Freundlich sorption is: $R = 1 + \frac{\rho_b}{\theta} a K_f C^{a-1}$. When the discretized transport equation is formulated for each node in the model, the result is a system of equations represented in matrix form (Eq. (4)). The continuous concentration variable (C) becomes a vector of concentrations at each finite difference cell ($\boldsymbol{c}$). The coefficient matrix $\boldsymbol{A}_c$ is a sparse, banded matrix that depends on the solute concentrations for simulations involving nonlinear sorption or reaction. Because the matrix $\boldsymbol{A}_c$ is a function of $\boldsymbol{c}$ and it is multiplied by the vector $\boldsymbol{c}$, Eq. (4) is a nonlinear equation. Also, because $\boldsymbol{c}^{t+1}$ is time dependent, $\boldsymbol{A}_c$ is also time dependent and is reformed at each time step using updated values of $\boldsymbol{c}$. The number of diagonals in $\boldsymbol{A}_c$ depends on the spatial dimensions of the simulation (1-D, 2-D, or 3D) as well as the treatment cross terms in the dispersion tensor. For the purposes of this study, a new MT3D-USGS feature that lumps cross-dispersion terms (which could also be omitted) into the right-hand-side vector is not used.

$$\boldsymbol{A}_c\boldsymbol{c}^{t+1} = \boldsymbol{b} \tag{4}$$

An important consideration in advection-dispersion modeling is the Peclet number (Pe), which is defined in Eq. (5).

$$Pe = \frac{|v|\Delta x}{D} \tag{5}$$

Where $|v|$ is the magnitude of seepage velocity of groundwater flow, Δx is the length of one model cell, and D is the magnitude of dispersion coefficient. The Peclet number is an indicator for the amount of advection relative to dispersion. Large Peclet numbers ($Pe > 2$) represent an advection-dominated simulation which can suffer from numerical errors (Zheng and Bennett, 2002). Simulations in this study are restricted to dispersion-dominated cases ($Pe < 1$) to avoid these problematic errors.

2.3. Model reduction

Model reduction of the advection-dispersion equations is achieved by projecting the full system of equations onto a lower dimensional subspace by the methods first presented for groundwater flow in Vermeulen et al. (2004a). In summary, a smaller system with fewer unknown variables is formed that captures most of the dynamics of the original system, as measured by the principal vectors obtained through singular value decomposition (SVD). The Intel Fortran preconditioned Jacobi SVD algorithm (https://software.intel.com/en-us/mkl-developer-reference-fortran-singular-value-decomposition-lapack-driver-routines) is used in this study. In order to build the reduced system, a collection of full-system 'snapshots' must be obtained. Then, truncated SVD is applied to the snapshots and Galerkin

Algorithm 1 Algorithm for selecting the interpolation indices z_j for $j = 1, \ldots, d$ (Stanko et al., 2016).

1. Construct a basis $D \in \mathbb{R}^{n \times d}$ from POD on snapshots of a nonlinear term
2. Select z_1 as the index of the largest element of d_1, the first column of D
3. For the remaining $j = 2, \ldots, d$ columns:
   a. Calculate $c = \left(Z^T[d_1, \ldots, d_j]\right)^{-1}\left(Z^T d_j\right)$
      Where $Z = \left[e_{z_1}, \ldots, e_{z_j}\right]$
   b. Compute the residual $r = d_j - Dc$
   c. Take z_j to be the index of $\|r\|_\infty$

projection is employed to reduce the dimension of the original system. In addition, a second set of snapshots is used to represent the nonlinearities of the model, which for this study is the entire matrix calculation: $A_c c^{t+1}$. SVD and Galerkin projection are both performed again on the nonlinear snapshots and the dual-reduced model is formed. In this section, these steps are explained in more detail.

2.3.1. Snapshot selection

Snapshots are defined as a full spatial representation of the system state at an instant of time. A selection of snapshots is needed for both POD and DEIM methods. For POD, snapshots of the vector c—obtained when Eq. (4) is solved by any of the solution techniques native to the MT3D-USGS software—are preserved at selected times and added to the snapshot set, Φ_c. For DEIM, snapshots of the nonlinear calculation in Eq. (4) ($A_c c^{t+1}$), which is equivalent the right-hand side vector b, are retained in Φ_b. The snapshot times are identical for Φ_c and Φ_b. The snapshot selection procedure includes selecting which simulation variables (e.g. aquifer parameters and boundary condition values) to use for each sample of the full model and the times at which the solution is added to the snapshot set. The performance of a projection-based reduced model is highly sensitive to the snapshot set used to construct the reduced basis (Siade et al., 2010).

2.3.2. Proper orthogonal decomposition

Proper orthogonal decomposition (POD) is a method used to decompose a matrix into orthogonal components. First, singular value decomposition is performed on Φ_c. Then a number of singular values that account for nearly all (e.g., 99% or 99.9%) of the matrix information (also called energy) can be selected and the remaining singular values are truncated and discarded. The percent energy criterion is used to define the number of singular values retained, which translates to the first reduced dimension, r. The matrix $P \in \mathbb{R}^{n \times r}$, with $r \ll n$, is composed of the eigenvectors corresponding to the r largest singular values. The full state space vector $c \in \mathbb{R}^{n \times 1}$ can now be approximated as Pc_r, where $c_r \in \mathbb{R}^{r \times 1}$. Substituting this approximation into Eq. (4) yields:

$$A_c P c_r^{t+1} = b \tag{6}$$

2.3.3. Galerkin projection

The Galerkin Projection technique involves the translation from full-model space to reduced model space. To achieve this reduction, Eq. (6) is premultiplied by P^T to obtain Eq. (7), which is a reduced system of equations (herein called the POD-reduced model). While the dimension of some calculations is reduced in the POD-reduced model of Eq. (7), the calculation $P^T A_c$ needs to be computed at each time-step (since the entries of A_c depend on the changing concentration field) and scales with the original full dimension of n.

$$P^T A_c P c_r^{t+1} = P^T b \tag{7}$$

2.3.4. Discrete empirical interpolation method

The discrete empirical interpolation method (DEIM) is a method used to capture nonlinear dynamics of a system of partial differential equations through a finite set of interpolation indices. The discrete empirical interpolation method is implemented specifically to reduce the nonlinear term's dependency on the full dimension of the original model, n. To approximate nonlinearities in a reduced space a nonlinear projection basis, D, is obtained via POD on Φ_b. The initial DEIM approximation (Eq. (8)) is made by approximating the nonlinear operation ($A_c c^{t+1}$) with a linear operation.

$$A_c c^{t+1} \cong D z \tag{8}$$

Where $z \in \mathbb{R}^{d \times 1}$ is a vector of unknown coefficients. Since Eq. (8) is overdetermined, only d equations are required to solve for z. The retained rows of the system are the interpolation indices that are selected through the process described in Stefanescu and Navon (2013). The selection algorithm for the interpolation indices chooses points that have the largest residual error when iteratively reconstructing the basis with an additional column of D in each iteration. Algorithm 1 shows the pseudocode for selecting the interpolation indices and the steps involved in the DEIM procedure.

To reformulate Eq. (8) as a well-determined system of equations, $Z \in \mathbb{R}^{n \times d}$ is defined as a diminished permutation matrix which retains only the d columns of a full permutation matrix ($d \ll n$) corresponding to the interpolation indices, d. Premultiplying Eq. (8) by Z^T (Eq. (9)) retains only the rows of A_C and D that correspond to interpolation points.

$$Z^T A_c c^{t+1} = Z^T D z \tag{9}$$

Eq. (9) can now be inverted to solve for z (Eq. (10)) and subsequently substituted back into Eq. (8) to obtain the final approximation of the nonlinear term (Eq. (11)). Finally, Galerkin projection can be applied again, as in Eq. (7), to achieve a new reduced model, herein called the POD-DEIM-reduced model (Eq. (12)).

$$z = \left[Z^T D\right]^{-1} Z^T A_c \, c^{t+1} \tag{10}$$

$$A_c c^{t+1} \cong D\left[Z^T D\right]^{-1} Z^T A_c c^{t+1} \tag{11}$$

$$P^T D\left[Z^T D\right]^{-1} Z^T A_c P c_r^{t+1} = P^T b \tag{12}$$

$(r \times n)(n \times d)[(d \times d)](d \times n)(n \times r)(r \times 1) = (r \times 1)$

Table 2
The values assigned to the 1-D MT3D-USGS transport model and the MODFLOW groundwater model.

Transport Model		Flow Model	
Cell size (Δx)	1 m	Cell size (Δx)	1 m
Cell size (Δz)	10 m	Cell size (Δz)	10 m
Simulation time	100 days	Simulation time	100 days
Stress periods (*nper*)	1	Stress periods (*nper*)	1
Time-steps (*nstp*)	100	Time-steps (*nstp*)	1
Time-step size (Δt)	1 day	Time-step size (Δt)	N/A (steady-state)
Initial concentration	1 g/m^3	Initial head	9.9 m
Mass-loading rate ($x = 30$)	200.0 g/day	Constant head ($x = 0$)	10 m
Bulk density	1000 g/m^3	Constant head ($x = 100$)	9 m
Dispersivity	10 m	Hydraulic conductivity ($K_x = K_y$)	25 m/day
Porosity	0.3	Specific Storage	N/A
Freundlich constant (K_f)	0.01 (m^3/g)$^{1/3}$	Source/Sink of water	0 m^3/day
Freundlich exponent	0.33		
Peclet number	0.025		

All calculations dependent on the dimension n ($\boldsymbol{P}^T\boldsymbol{D}[\boldsymbol{Z}^T\boldsymbol{D}]^{-1}$) can be precomputed and the precomputation of $[Z^TD]^{-1}$ is executed with LU decomposition. The final POD-DEIM-reduced model (Eq. (12)) is solved for c_r^{t+1} at each time step entirely within the reduced dimension. In other words, there are no nonlinear operations that must be carried out in the full n-space during the simulation and the complexity of the POD-DEIM-reduced model solution scales only with dimensions r and d. Note that since $\boldsymbol{A}_c$ is a sparse matrix that results from finite difference discretization, the complexity of $\boldsymbol{A}_c\boldsymbol{P}$ scales with the dimension r, not n.

2.4. Error and uncertainty

The error for any reduced model is henceforth defined as the difference between the original full-model solution and the reduced model solution. This error is calculated for both the concentration solution in the full model dimension as well as the result of the nonlinear operation $\boldsymbol{A}_c\boldsymbol{c}$, which is the same as the vector $\boldsymbol{b}$ for the governing equation under consideration. Absolute error is presented in concentration units. Root mean squared errors (RMSE), and normalized root mean squared error (NRMSE) are calculated for each case so the errors can be weighted by the span of concentration values (Eq. (13)).

$$NRMSE = \frac{\|full - reduced_2\|}{\sqrt{n} * (c_{max} - c_{min})} = \frac{RMSE}{(c_{max} - c_{min})} \tag{13}$$

Where $\|\cdot\|_2$ is the Euclidean norm.

To account for various numerical inaccuracies, a statistical experiment is designed such that uncertain components of the reduced modeling methodology are varied randomly to assess their significance. This research employs a random draw from a uniform distribution of mass-loading rates and a random log-normal hydraulic conductivity field. The field was generated with the Python package pyEMU (White et al., 2016) using ordinary kriging and an exponential variogram (range = 304 and contribution = 1.0). The accuracy of the reduced model always depends on the snapshot set and number of principal vectors retained after truncation. Given that, this uncertainty experiment shows the range of accuracies attainable with an already constructed reduced model, assuming the snapshot set is sufficient. An optimal snapshot set might achieve superior accuracy, but this is beyond the scope of this study.

3. One-dimensional test case

The first test of the POD-DEIM methodology was implemented within MT3D-USGS and tested on a simple one-dimensional (1-D) model. Eq. (14) describes the 1-D transport governing equation as modified from Eq. (2), where change in groundwater storage is zero ($q_s' = 0$) for steady flow, mass-loading (q_c) replaces the flux term ($q_s c_s$), and the dispersion coefficient (D) is treated as constant. In this 1-D model, the aquifer is assumed to me homogeneous and isotropic.

$$R\frac{\partial c}{\partial t} = -v_x\frac{\partial c}{\partial x} + D\frac{\partial^2 c}{\partial x^2} + q_c - \lambda_1\theta c - \lambda_2\rho_b\bar{c} \tag{14}$$

3.1. 1-D model design

The 1-D model consists of 100 finite difference cells, each 1 m in length—in the parlance of model terms, these are represented as one row by 100 columns. Each cell has a depth of 10 m and constant head cells are assigned at the left, $h(x = 0) = 10.0\ m\ \forall t$, and right, $h(x = 100) = 9.0\ m\ \forall t$, boundaries. The flow field is simulated as steady-state to isolate system changes due to solute concentration only. The simulation runs for 100 days in one model stress period and a time step of 1 day. Initial concentration is specified as 1.0 g/m^3 and a source (mass loading) takes place at $x = 30$. Table 2 summarizes the model setup with additional parameter settings.

The concentrations in the simulation represent a solute plume that has formed by way of both advection and dispersion after 100 days of mass loading. The plume at 100 days is shown in Fig. 1 for the full model. After 100 days, concentrations range from the minimum initial concentration of 1.0 g/m^3 to a maximum of about 62 g/m^3 at the solute source ($x = 30\ m$).

3.2. 1-D reduced model

To mitigate the potential effect of snapshot selection on the reduced model solution, a sufficient number of snapshots need to be used. Snapshots cannot be placed too far apart or they might misrepresent the nonlinear dynamics of the system. For this problem it was found experimentally that taking snapshots every 10 days achieved a good compromise between these objectives. Snapshots are thus taken every 10th time step for each variation of model forcings; the sole forcing in this case is the mass-loading rate (q_c). To achieve the goal of the reduced model effectively solving for concentration with varying q_c, snapshots are taken for a range of mass-loading rates: (25, 75, 100, 300, 500). Since there are 21 snapshots in each simulation, there are a total of 105 snapshots in each snapshot set. One snapshot set, $\boldsymbol{\Phi}_c$, is composed of solute concentration vectors ($\boldsymbol{c}$) at each time step; the other, $\boldsymbol{\Phi}_b$, is composed of the right-hand side vector ($\boldsymbol{b}$) for each time step.

A basis is generated for each of the snapshot sets ($\boldsymbol{\Phi}_c$ and $\boldsymbol{\Phi}_b$) using truncated SVD. For the POD basis, the reduced dimension is specified (after performing SVD on $\boldsymbol{\Phi}_c$) by truncating the singular values at a percent energy of 99.95%. The result is a basis ($\boldsymbol{P}$) with a reduced dimension of $r = 18$. For linear calculations only, this would represent a dimension reduction from 100 to 18. For the nonlinear basis ($\boldsymbol{D}$), the reduced dimension is specified directly as $d = 42$ and the 42 singular vectors associated with the 42 largest singular values are thus retained

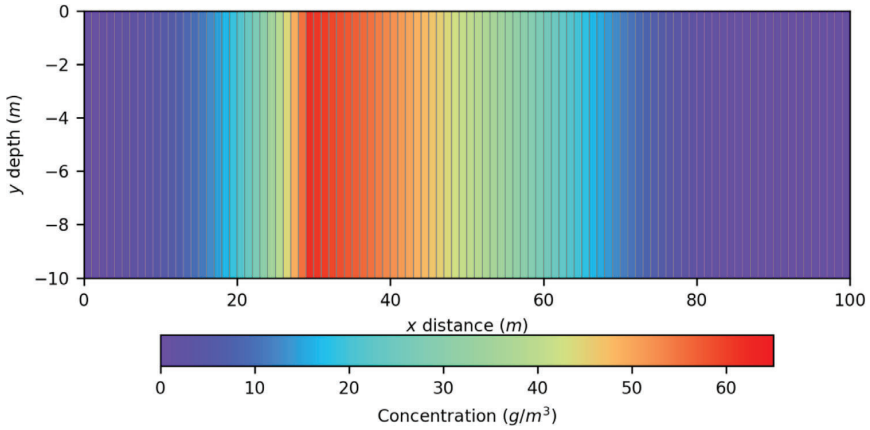

Fig. 1. The 1D test case full model solute concentrations after 100 days.

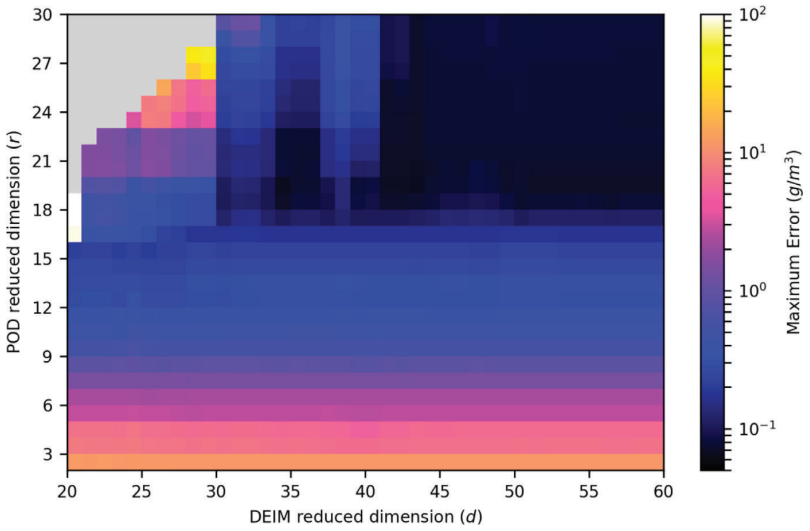

Fig. 2. A heatmap to show the combinatorial search over the two reduced dimensions, r, and d, with color representing the maximum error between the full model and the reduced model with each unique combination of reduced dimensions (For interpretation of the references to color in this figure legend, the reader is referred to the web version of this article .).

from truncated SVD on $\mathbf{\Phi}_b$. For nonlinear calculations, this represents a dimension reduction from 100 to 42. The combination of reduced dimensions of $r = 18$ and $d = 42$ was found experimentally by performing a combinatorial search and selecting the combination that yielded small maximum error while keeping the reduced dimensions small. Results of this search are shown in Fig. 2. It is evident that good solutions (maximum error near 0.1 g/m^3) are available with any combination of POD reduced dimensions (r) greater than 18 and DEIM reduced dimensions (d) greater than 42.

3.3. 1-D result

Initial results related to the performance of the reduced model are compiled for a mass-loading rate of $q_c = 200\ g/m^3$. Monitoring locations were applied at $x = 20,\ 40,\ 60$ and $80\ m$ to capture the accuracy at various extents of the solute plume. A single full model run was evaluated to determine reference concentrations for reduced model comparison. Breakthrough curves for solute concentration over time matched well for the reduced model. Fig. 3 shows the breakthrough curve comparisons for the four monitoring locations.

Since the reduced model's concentrations are very close to the full model (errors on the order of 1%), the reduced model plume is visually indistinguishable from the full model plume. Therefore, the reduced model result is presented as a difference in concentration between the full and reduced model ($\boldsymbol{c}_f - \boldsymbol{c}_r$). On the left side of Fig. 4, the error can be seen propagating over space and time but never exceeds 0.1 g/m^3. The oscillatory behavior of the error is common for projection-based reduced models and it is not problematic if the magnitude of the error is consistently below an acceptable threshold. The locations of the maximum error (0.07 g/m^3) is located near the source location ($x = 30\ m$) during the beginning of the simulation. On the right side of Fig. 4, the distribution of concentrations over the entire spatial domain at 50 and 100 days is shown to be very similar for the full and reduced model. The errors are all acceptable for models intended to be quick approximations. Moreover, the reduced model produced good solutions for a range of mass loading rates and the mass budget at each time step, as well as the cumulative mass budget, confirm that mass is being conserved.

Analysis of reduced model error in the 1-D case can help direct the implementation of POD-DEIM in more complex cases. The location and timing of the errors reveals the performance of the reduced model at the times and locations that are of specific interest to the modeler. For instance, the modeler may be more interested in capturing the peak concentration at a specific point, in which case, the breakthrough curves of Fig. 3 would be most important. Conversely, it may be more important

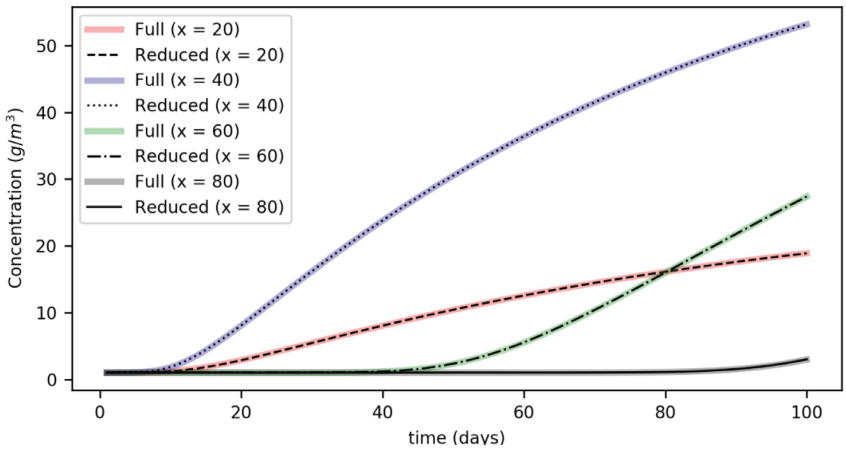

Fig. 3. The accuracy of the reduced model with respect to the full model for concentration breakthrough curves at $x = 20$, $x = 40$, $x = 60$, and $x = 80$.

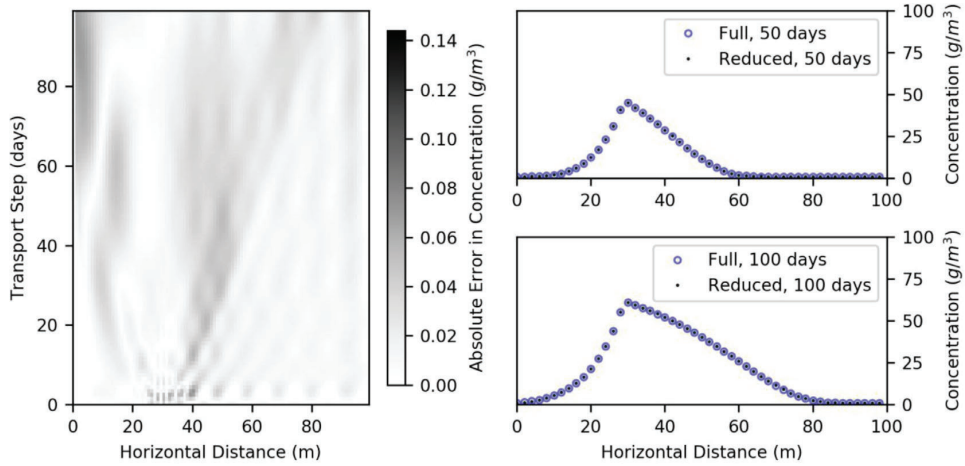

Fig. 4. The POD-DEIM ($r = 18$, $d = 42$) reduced model error shown for absolute error over all time (left) and by comparing simulated concentrations for the full and reduced model at snapshots for 50 days (top right) and 100 days (bottom right).

Table 3
Various error metrics compared for the POD ($r = 18$) and the POD-DEIM ($r = 18$, $d = 42$) reduced models. Minimum and maximum concentrations, absolute errors as defined by the full model minus the reduced model, root mean squared error (RMSE), and normalized root mean squared error (NRMSE), are all within acceptable values. All units are g/m^3 except NRMSE, which is dimensionless.

Metric	Full	POD only	POD-DEIM
min conc.	1.0	1.0	1.0
max conc.	61.64	61.64	61.64
abs. error min	–	0.0	0.00
abs. error max	–	0.08	0.07
RMSE	–	0.03	0.02
NRMSE	–	0.36	0.31

to model the overall mass of solute in a plume, in which case overall average error metrics would suffice. A summary of error metrics for the 1-D test case are in Table 3. For this case, both high and low concentrations match well throughout the domain and all error statistics are within acceptable ranges of numerical approximations. In comparison, the errors are slightly larger with the traditional POD approach, which doesn't address the nonlinearity.

4. Two-dimensional test case

The methodology is next applied to a regional-scale two-dimensional (2-D) model. The model is designed such that complexities are introduced only to sufficiently represent a realistic problem scale and not to accurately represent any specific real-world conditions. The 2-D snapshot selection, reduced basis construction, and reduced model evaluation are presented in this section.

4.1. 2-D model design

The 2-D model simulates a contaminant leak and the resulting plume migration. The model domain is 9300 m by 14,500 m and is composed of one layer, 144 rows and 92 columns, creating a full model dimension of 13,248 cells. The single layer has a depth of 100 m and each cubic cell is 100 m on each side, representing a volume of 10^6 m^3 of porous media. The contaminant leaks over a horizontal extent of 2000 m (at $y = 4$, 000 m and from $x = 4$, 000 m to$x = 6$, 000 m). The model runs for 5000 days with a specified constant mass-loading rate for each cell simulating the leak. The solute plume migrates down the hydraulic gradient toward a well field composed of four extraction wells. For the flow solution, the injection rate of the contaminant leak is 100 m^3/day and the extraction rate is 1000 m^3/day for all of the wells in the well field, both implemented with the MODFLOW well package (WEL). The flow field is deter-

mined by a single steady-state MODFLOW solution with constant head boundaries (CHD) to the north (40 m) and to the south (4 m) and a drain (DRN) set to 4 m in the lower left corner. The flow model features (CHD, DRN, and WEL) are shown in Fig. 5a along with the concentration plume at the end of the simulation. Hydraulic head contours of the steady flow field are shown in Fig. 5b along with a randomly generated hydraulic conductivity field (using ordinary kriging and an exponential variogram with range = 304 and contribution = 1.0). Additional model parameter values are specified in Table 4. It is assumed that the transport parameters are homogeneous and independent of the variations in hydraulic conductivity. Nonlinear sorption parameters were chosen to introduce a reasonable amount of contaminant retardation that increases nonlinearly as concentration increases according to the Freundlich isotherm.

4.2. 2-D reduced model

The snapshot selection for the 2-D test case involved substantial trial and error. Snapshots must be spaced far enough apart to capture changes in concentration substantially larger than model errors to avoid incorporating numerical noise into the basis. Conversely, snapshots must not be too far apart or a smooth dynamic response might not be captured. for the 2-D model, this balance was achieved experimentally and snapshots were taken every 6 days. For the reduced model to be robust with respect to the magnitude of concentrations, snapshots were taken for several simulations with various mass-loading rates. Altogether, five simulations were run at various mass-loading rates (1000, 1100, 1200, 1300 and 1500 g/day) intended to span a range of uncertainty in the boundary condition. 835 snapshots were taken for each simulation for a total of 4175 snapshots. The large snapshot set was devised to avoid the well-known issue of reduced model sensitivity to snapshot selection scheme. With an optimal snapshot selection algorithm, it is likely that a much smaller snapshot set would be sufficient.

For the first reduced basis ($\boldsymbol{P}$) that represents the POD-based reduced model, the dimension of the system was reduced from 13,248 to 10 ($r = 10$), capturing 99.5% of the system energy while reducing the dimension of the system by three orders of magnitude. For the second, nonlinear basis ($\boldsymbol{D}$), the DEIM-based reduced model used a reduced dimension of $d = 286$, capturing over 99.98% of the nonlinear system energy while reducing the dimension of the nonlinear calculations by two orders of magnitude. Since a combinatorial search for an optimal pair of reduced dimensions for the 2-D model was not feasible for the entire reduced dimension space, an abbreviated search was conducted and is shown in Fig. 6. Fig. 6 addresses the sensitivity of the reduced model accuracy to the selection of POD and DEIM basis vectors. Beyond a re-

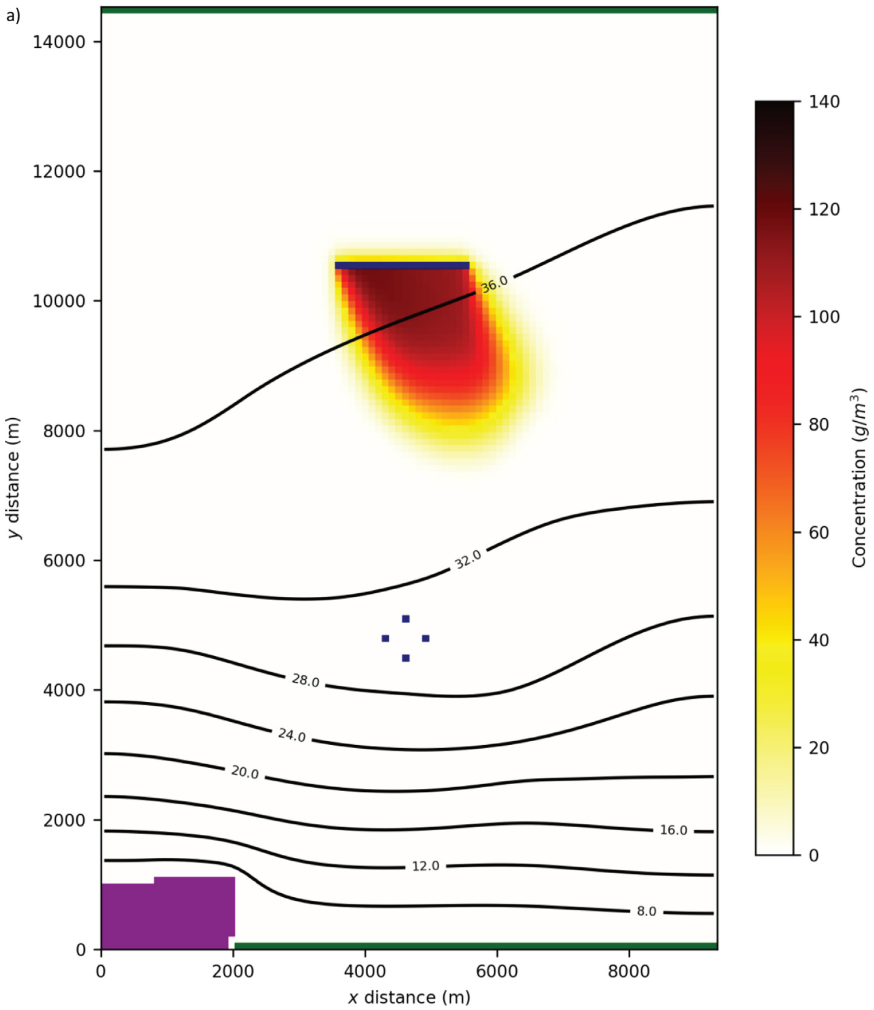

Fig. 5. a) The 2-D model domain showing the concentration plume after 5000 days (MODFLOW well cells shown in blue; constant head cells in green; and drain cells in purple) and b) the contours of hydraulic head and the randomly generated hydraulic conductivity (K) field.

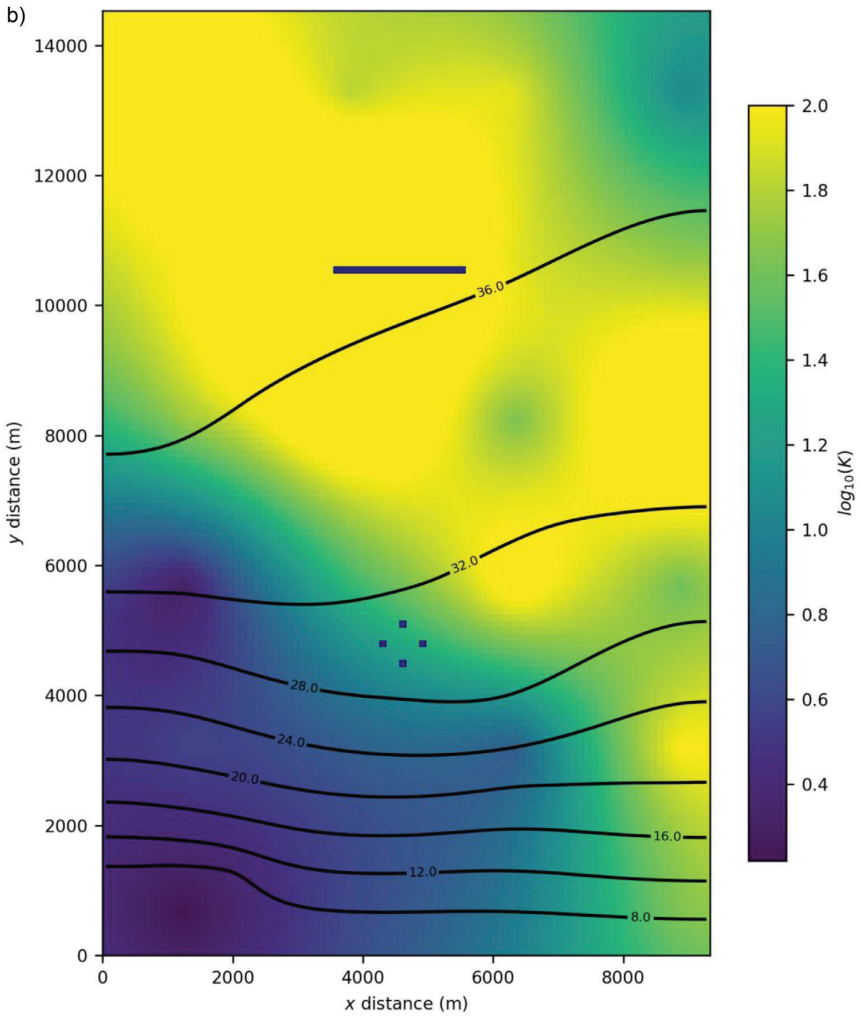

Fig. 5. Continued

Table 4
The values assigned to the 2-D MT3D-USGS transport model and the MODFLOW groundwater model.

Transport Model		Flow Model	
Cell size ($\Delta x = \Delta y$)	100 m	Cell size (Δx)	100 m
Cell size (Δz)	100 m	Cell size (Δz)	100 m
Simulation time	5000 days	Simulation time	5000 days
Stress periods (*nper*)	1	Stress periods (*nper*)	1
Time-steps (*nstp*)	5000	Time-steps (*nstp*)	1
Time-step size (Δt)	1 day	Time-step size (Δt)	Steady-state
Initial concentration	1 g/m^3	Initial head	10 m
Mass-loading rate	Range(1000–1500) g/day	Constant head ($y = 0$ m)	40 m
Bulk density	1000 g/m^3	Constant head ($y = 14,500$ m)	4 m
Dispersivity	57 m	Hydraulic conductivity ($K_x = K_y$)	Range(0.01 to 100) m/day
Porosity	0.2	Specific Storage	n/a
Freundlich constant (K_f)	0.001 (m^3/g)$^{1/3}$	Source/Sink of water:	
Freundlich exponent	0.33	leak	100 m^3/day
Peclet number (max *Pe*)	0.7	Well field	4 wells at −1000 m^3/day each

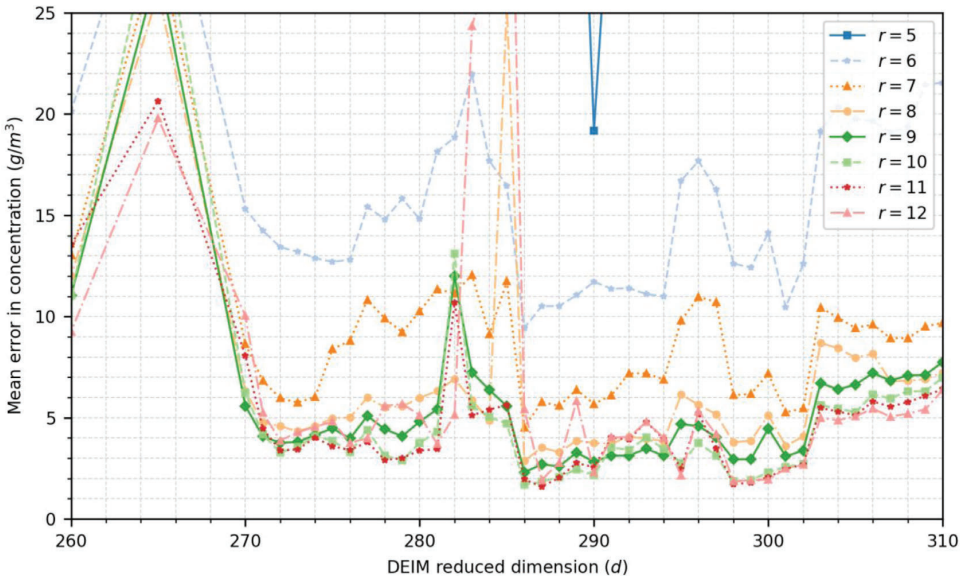

Fig. 6. An abbreviated search over the reduced dimension space to find appropriate combinations of dimensions p and d.

duced dimension of $r = 12$ for the POD step, there is no further improvement in accuracy regardless of the number of DEIM points used. The reduced dimensions were determined experimentally to be the smallest such dimensions that produced a reduced model solution with the lowest possible error.

4.3. 2-D result

The POD-DEIM reduced model performance is demonstrated on a simulation with a mass-loading rate of 1250 g/day. The concentration distribution of the full model plume after 5000 days is shown in Fig. 5. Concentration contours for both the full model and the reduced model are compared in Fig. 7. In the context of the model domain, the full and reduced concentration contours match very well. For a closer look at the change in concentration over time, four observation locations—positioned in (row, column): (44, 38); (49, 48); (53, 57); and (60, 53); shown in Fig. 7—produce breakthrough curves for the full and reduced model (Fig. 8). Slight errors in concentration are evident by the deviation of the reduced model (black lines) curves from the center line of the full model (colored lines) curves. With respect to the magnitude of the full model concentrations being approximated, the maximum errors are less than 2%.

A more complete picture of the error can be shown by comparing the snapshots collected from both the full and reduced models. The RMSE for concentration in each model cell captured in the snapshots is presented in Fig. 9. The largest errors occur in a row of cells just below the source of the mass loading, but these cells still have an RMSE less than 2 g/m^3. For the nonlinear snapshots, the result (Fig. 10) is similar but due to the large magnitude of values in the snapshots it is presented in terms of NRMSE. The locations of the 286 interpolation points are also shown in Fig. 10 as black dots. Most of the points are clustered around the plume location and some are scattered along the trajectory of the plume. One point is kept slightly above the mass loading boundary, which represents the upgradient background concentration.

The POD-DEIM reduced model was also tested on 50 simulations with randomly generated mass-loading rates that span those included in the snapshot set, i.e., 1000–1500 g/m^3. Both the full model and the POD-DEIM reduced model with $r = 10$ and $d = 286$ were run and compared for each sample. The statistics of errors in the snapshot sets, compiled over all 50 samples and compared to the single reduced model, are shown in Table 5. The mean NRMSE and percent error are similar for both sets of snapshots. The mean RMSE over the entire model domain is also captured for each snapshot time and presented in Fig. 11a.

Nearly 100% of all snapshot times have an RMSE less than 1 g/m^3, with a maximum RMSE of 0.42 g/m^3. In Fig. 11b, the maximum reduced error for each of the 50 samples is compared to the maximum simulated concentration, which reflects the mass-loading rate imposed. The samples with the lowest error were near the middle of the concentration range incorporated in the snapshots. Additionally, there is larger error associated with larger concentrations, which could be due to the larger mass-loading interval used between snapshots taken for 1300 and 1500 g/day.

5. Discussion

Selection of the reduced dimensions r and d for the 1-D model show that the reduction potential for such a simple model is limited. A dimension reduction from 100 to 42 implies 42 out of a possible 100 interpolation points are used to obtain a good reduced model (Fig. 2). Conversely, for the 2-D model, a dimension reduction from 13,248 to 286 implies 286 out of a possible 13,248 (about 2%) interpolation points are used for an accurate 2-D reduced model. Considering that the solute plume in the 1-D model covers a significant portion of the model domain, the amount of the model domain that needs to be incorporated into the POD-DEIM reduced model via the reduced dimension d may depend on the spatial extent of the changing concentrations. Though the dynamics between the specification of the two reduced dimensions is model-specific, it is clear for the 1-D test case that $d \geq 42$ is necessary for accurate reduced model solutions. Given $d \geq 42$, a range of values for r produce acceptable error and that error generally decreases monotonically with increasing r. While the 1-D model does show the concept of POD-DEIM model reduction can work with acceptable error for a nonlinear solute transport problem, in practice there would never be a need for a reduced version of such a simple model, thereby necessitating a more complex 2-D test case.

The results of the 2-D test case demonstrate the effectiveness of the POD-DEIM reduced model on a regional-scale solute transport

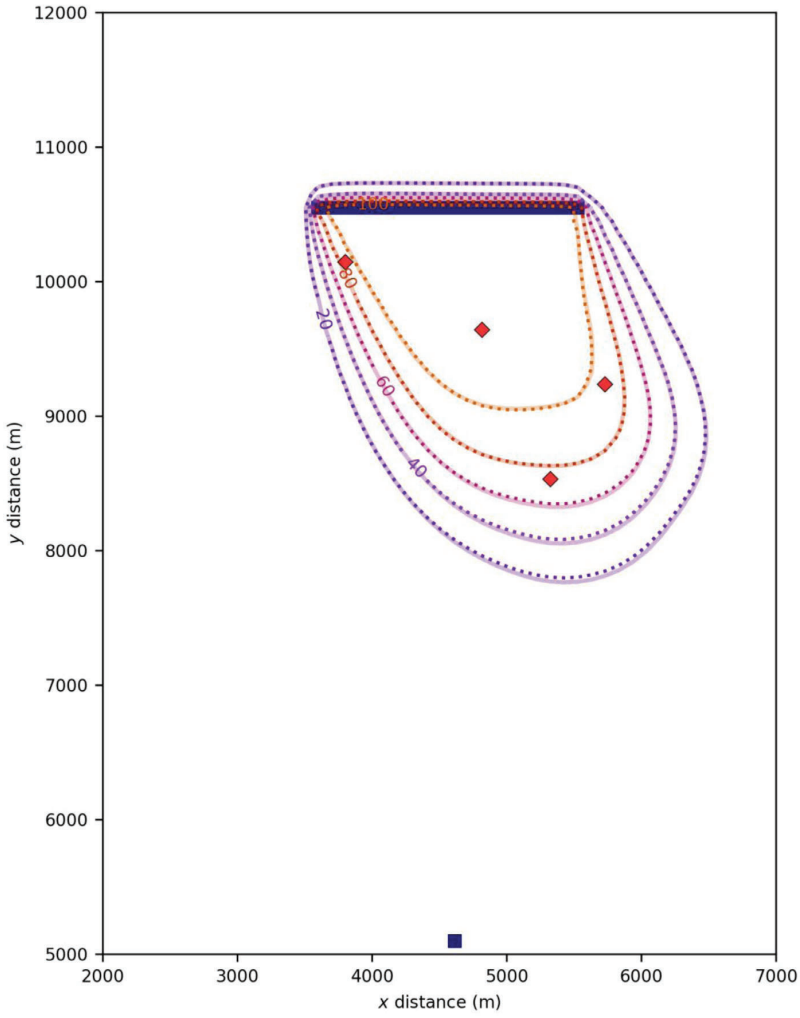

Fig. 7. Contours of concentration (g/m^3) at the end of the simulation (5000 days) for the full model (solid lines) and the POD-DEIM reduced model (dotted lines). MODFLOW wells are shown as blue rectangles and concentration observation locations as red diamonds.

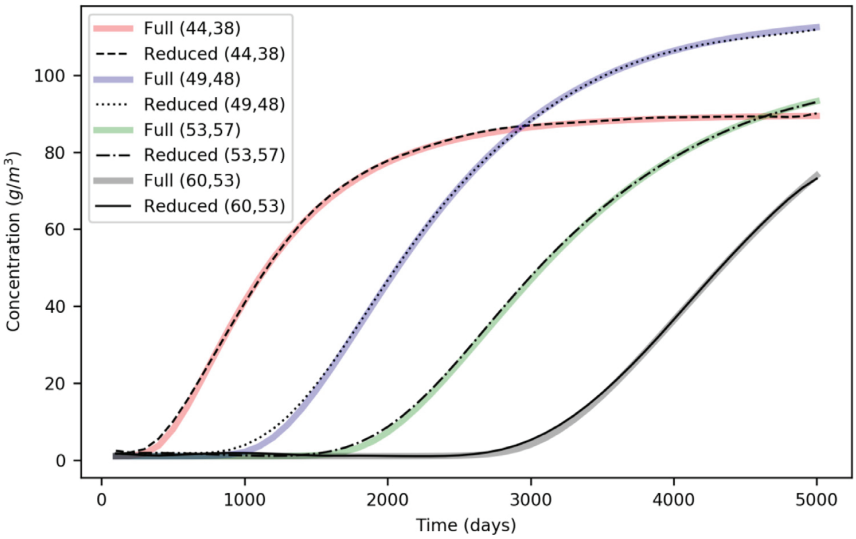

Fig. 8. Concentration breakthrough curves at three observation locations for both the full model and the POD-DEIM reduced model with the (row, column) location of the observation.

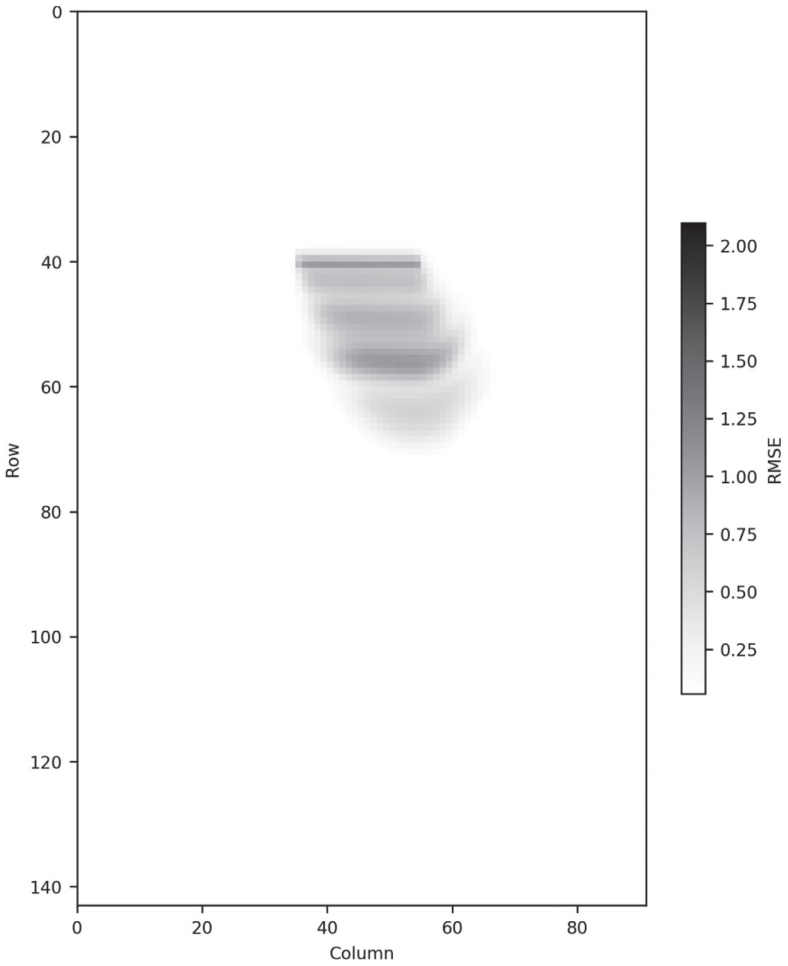

Fig. 9. The RMSE of the concentration snapshots for the POD-DEIM reduced model.

Table 5
Error statistics for the single reduced model (with mass loading of 1250 g/day) and 50 samples of reduced models with random mass loading rates.

Concentration snapshots	Full model max. concentration (g/m^3)	Max. absolute error (g/m^3)	Mean RMSE	Mean NRMSE	Percent error (%)
single model	118.25	2.36	0.16	0.001	2.00
50 samples min.	95.53	2.36	0.15	0.001	1.92
50 samples max.	141.61	11.71	0.42	0.005	8.27
50 samples mean	118.37	105.21	0.27	0.002	4.38

Nonlinear snapshots	Full model max (absolute value)	Max. absolute error	Mean RMSE	Mean NRMSE	Percent error (%)
single model	−25,967,263	547,913	39,254	0.0015	2.11
50 samples min.	−30,873,604	546,429	37,099	0.0014	2.03
50 samples max.	−21,179,877	2502,914	99,655	0.0047	8.12
50 samples mean	−25,967,529	1134,842	62,273	0.0025	4.35

simulation with nonlinear sorption. The reduced dimensions were three orders of magnitude less than the full dimension for the initial POD on the snapshots of concentration and two orders of magnitude less than the full dimension for DEIM on the nonlinear snapshots. Though the selection of the reduced dimensions is problem dependent and requires some trial and error, at least 99.9% energy is preserved when constructing both the POD and the DEIM bases ($\boldsymbol{P}$ and $\boldsymbol{D}$). The location of the DEIM points are automatically chosen and demonstrate good coverage of the solute plume's spatial extent. As expected, points corresponding to locations with negligible changes in concentration are not used. It was found that adding additional DEIM points beyond 286 did not significantly reduce the error (Fig. 6) as they may be providing too much redundant (linearly dependent) information.

The POD-DEIM reduced models developed with the methods of this research are robust to uncertainties in mass-loading rates and the underlying flow field. This means that if the exact leakage rate of a contaminant was unknown, any number of mass-loading rates (within the range of those used to construct the snapshot set) can be simulated and the reduced model would perform well. The analysis of 50 random samples of mass-loading rates shows that accuracy is best near the middle of the

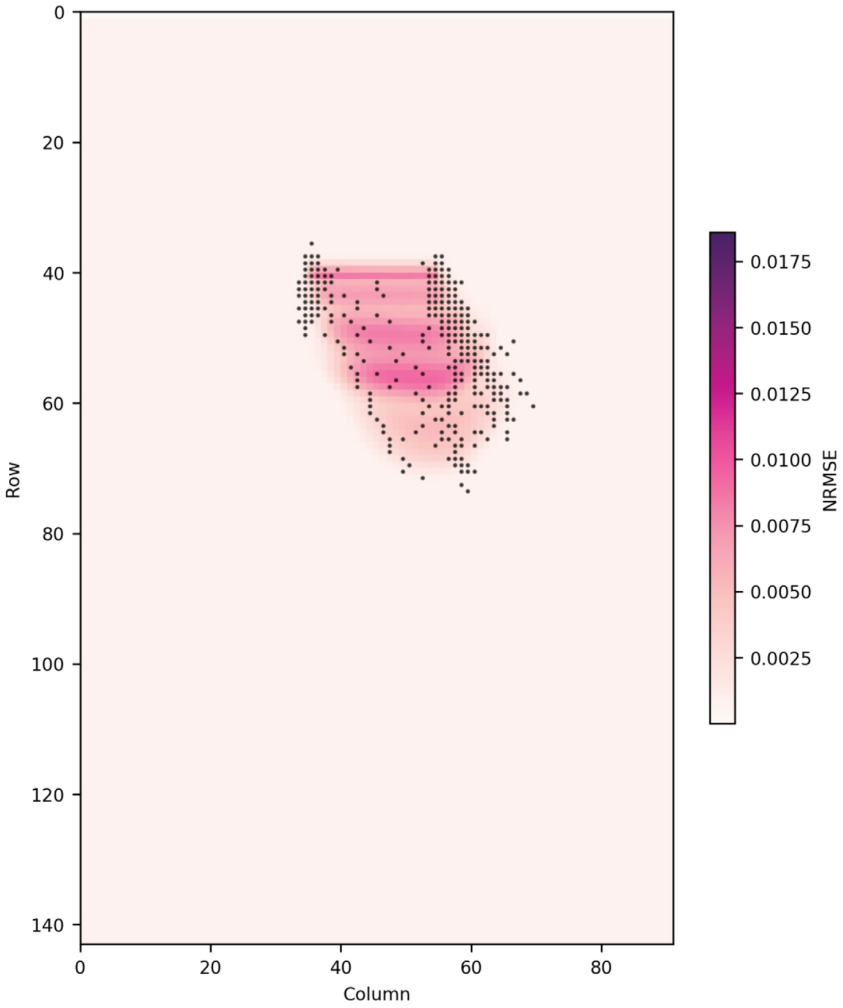

Fig. 10. The NRMSE of the nonlinear snapshots for a POD-DEIM reduced model with 286 interpolation points (shown as black dots).

range used to construct the snapshot set (Fig. 11b); therefore, the snapshot set should be designed to adequately bracket the range of uncertainty. Uncertainty in the steady flow field was examined by generating a stochastic hydraulic conductivity field. The variation in magnitude and direction of the velocity vectors presents additional complexity to the solute transport model. The sufficient accuracy of the reduced model under these conditions implies that the automatic selection of DEIM points works to capture both advection and dispersion in various directions. Additional sources of uncertainty could be captured in the snapshot sets by varying other model inputs, such as transport parameters.

The results for both the 1-D and 2-D models exhibit high sensitivity to the snapshot set. The numerical results for each reduced model substantially depend on what is captured in the snapshot set. The snapshot set size is determined by a) how many snapshots are taken for each simulation; and b) how many simulations are performed over the range of stresses (mass-loading rate in this case) being captured. The sensitivity is also related to the values chosen for the stresses in each simulation. If the magnitude of these stresses span a large range, there may be a need for more simulations in the snapshot set than if they span a small range. These findings related to the snapshot set sensitivity highlight the potential benefit of an optimal snapshot selection method. However, good reduced model performance has been demonstrated even without optimal snapshots, suggesting that an optimal snapshot selection could only further improve the performance.

Rudimentary timing analysis shows that the POD-DEIM reduced model is always faster than the full model. However, due to optimized solver options for the full model and a generic reduced model solver, timing of the full and reduced models is not directly comparable. Even so, the reduced model for the 2-D test case reduces run time to an average of about 3.5 min, compared to about 10 min for the full model (performed on an Intel(R) Core(TM) i7 @ 2.8 GHz). It is important to note that for these experiments, it is the order of magnitude of the problem dimensions that signifies the substantial improvement of the reduced model with respect to the full model. The speedup of the reduced model is also limited by the overhead of the software, such as extensive file read and write routines. To account for this, CPU time was also compared for the cumulative time spent in the full model solver (419 s) and the generic reduced model solver (22 s) for a speedup of about 95%. In contrast, 0.14 s of CPU time were needed for the DEIM calculations in Eq. (12) that are precomputed once for each simulation. If an optimal solver was designed for the reduced model, as it was for the full model (Zheng and Wang, 1999), reduced model runtime could be substantially reduced. While optimizing the code for speed was not the focus of this research, the successful reduced model implementation within

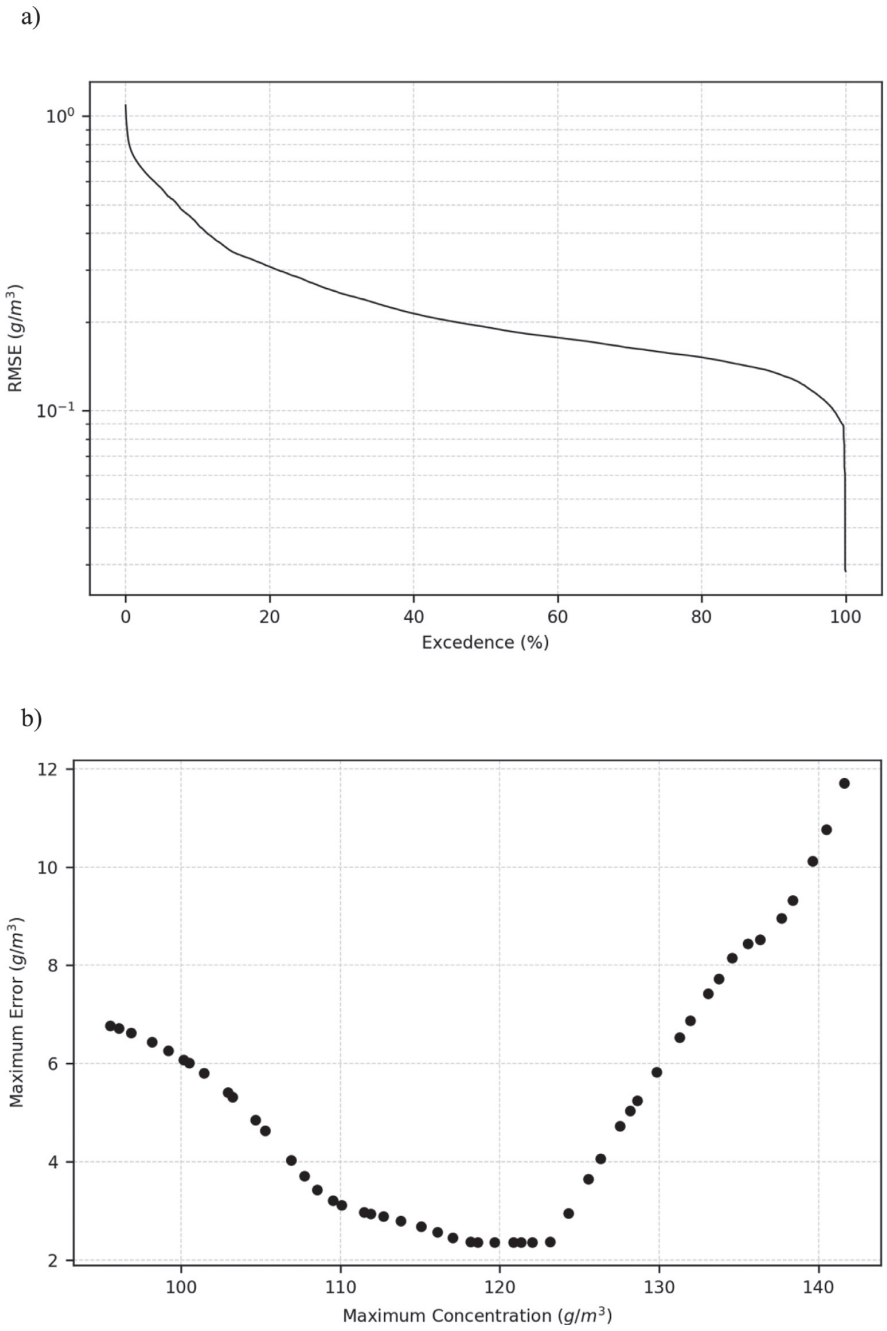

Fig. 11. a) The percent exceedance for the RMSE of the entire model domain at each snapshot time for each of the 50 samples; and b) The maximum error in concentration for each of the 50 samples as a function of the maximum simulated concentration.

commonly used software provides an avenue for broader applications of POD-DEIM. Primarily, the reduction of the problem dimensions by two and three orders of magnitude presents a major step toward faster nonlinear solute transport simulations.

6. Conclusion

In conclusion, this research demonstrates the feasibility of using POD and DEIM to reduce a solute transport model with nonlinear sorption and largely dispersive behavior (low Peclet number). While the application of POD-DEIM to this type of solute transport is the primary contribution of this work, a secondary contribution is the modification of the MT3D-USGS software. The implementation of this research within the MT3D framework provides flexibility for the application of POD-DEIM since many solute transport models that have been published to date utilize that software. The methods were tested on a simple 1-D model and a more complex, heterogenous 2-D model. An explicit trade-off between the two reduced dimensions was presented for each case. For the regional scale 2-D model, the reduced dimensions were three and two orders of magnitude less than the full model dimensions for the POD and

DEIM reduction routines, respectively. While the speedup of the reduced model is limited by the overhead of the software, this dimension reduction for nonlinear solute transport models is demonstrated for the first time. The application of the reduced modeling methodology also demonstrated a sensitivity to snapshot selection, but accurate reduced models were produced even without an optimal snapshot selection. Overall, this study represents a step toward being able to reduce very large, complex, regional groundwater flow and solute transport simulations. Future research in this field might involve reduced modeling strategies for the combination of nonlinear groundwater flow and nonlinear solute transport, since this is the common case for many modern models used for planning and management purposes.

Acknowledgments

We wish to thank the four anonymous reviewers for their thoughtful and constructive reviews.

This material is based on work supported by NSF under award EAR-1314422. Partial support also was provided by an AECOM endowment.

References

Asher, M.J., Croke, B.F.W., Jakeman, A.J., Peeters, L.J.M., 2015. A review of surrogate models and their application to groundwater modeling. Water Resour. Res. 51, 5957–5973. https://doi.org/10.1002/2015WR016967.

Bedekar, V., Morway, E.D., Langevin, C.D., Tonkin, M., 2016, MT3D-USGS version 1: A U.S. Geological Survey release of MT3DMS updated with new and expanded transport capabilities for use with MODFLOW: U.S. Geological Survey Techniques and Methods 6-A53, 69 p., http://dx.doi.org/10.3133/tm6A53.

Boyce, S.E., Nishikawa, T., Yeh, W.W.-G., 2015. Reduced order modeling of the Newton formulation of MODFLOW to solve unconfined groundwater flow. Adv. Water Resour. 83, 250–262. https://doi.org/10.1016/j.advwatres.2015.06.005.

Boyce, S.E., Yeh, W.W.-G., 2014. Parameter-independent model reduction of transient groundwater flow models: application to inverse problems. Adv. Water Resour. 69, 168–180. https://doi.org/10.1016/j.advwatres.2014.04.009.

Chaturantabut, S., Sorensen, D.C., 2011. Application of POD and DEIM on dimension reduction of non-linear miscible viscous fingering in porous media. Math. Comput. Model. Dyn. Syst. 17, 337–353. https://doi.org/10.1080/13873954.2011.547660.

Chaturantabut, S., Sorensen, D.C., 2010. Nonlinear model reduction via discrete empirical interpolation. SIAM J. Sci. Comput. 32, 2737–2764.

Dimitriu, G., Navon, I.M., Ştefănescu, R., 2014. Application of POD-DEIM Approach for Dimension Reduction of a Diffusive Predator-Prey System with Allee Effect. In: Lirkov, I., Margenov, S., Waśniewski, J. (Eds.). Large-Scale Scientific Computing. LSSC 2013. Lecture Notes in Computer Science, vol. 8353. Springer, Berlin, Heidelberg.

Hanson, R.T., Boyce, S.E., Schmid, W., Hughes, J.D., Mehl, S.M., Leake, S.A., Maddock, T., III, Niswonger, R.G., 2014, One-Water Hydrologic Flow Model (MODFLOW-OWHM): U.S. Geological Survey Techniques and Methods 6A51, 120 p., http://dx.doi.org/10.3133/tm6A51.

Harbaugh, A.W., 2005. MODFLOW-2005, The U.S . Geological Survey Modular Ground-Water Model — the Ground-Water Flow Process. In: MODFLOW-2005, The U.S . Geological Survey Modular Ground-Water Model — the Ground-Water Flow Process, p. 253.

Li, X., Chen, X., Hu, B.X., Navon, I.M., 2013. Model reduction of a coupled numerical model using proper orthogonal decomposition. J. Hydrol. 507, 227–240. https://doi.org/10.1016/j.jhydrol.2013.09.011.

Li, X., Hu, B.X., 2013. Proper orthogonal decomposition reduced model for mass transport in heterogenous media. Stoch. Environ. Res. Risk Assess. 27, 1181–1191. https://doi.org/10.1007/s00477-012-0653-2.

McPhee, J., Yeh, W.W.-G., 2008. Groundwater management using model reduction via empirical orthogonal functions. J. Water Resour. Plan. Manag. 134, 161–170. https://doi.org/10.1061/(ASCE)0733-9496(2008)134:2(161).

Pasetto, D., Putti, M., Yeh, W.W.-G., 2013. A reduced order model for groundwater flow equation with random hydraulic conductivity: application to monte carlo methods. Water Resour. Res. https://doi.org/10.1002/wrcr.20136, n/a-n/a.

Rizzo, C.B., de Barros, F.P.J., Perotto, S., Oldani, L., Guadagnini, A., 2018. Adaptive POD model reduction for solute transport in heterogeneous porous media. Comput. Geosci. 22, 297–308. https://doi.org/10.1007/s10596-017-9693-5.

Robinson, B.A., Lu, Z., Pasqualini, D., 2012. Simulating solute transport in porous media using model reduction techniques. Appl. Math. 3, 1161–1169. https://doi.org/10.4236/am.2012.310170.

Siade, A.J., Putti, M., Yeh, W.W.-G., 2012. Reduced order parameter estimation using quasilinearization and quadratic programming. Water Resour. Res. 48. https://doi.org/10.1029/2011WR011471.

Siade, A.J., Putti, M., Yeh, W.W.-G., 2010. Snapshot selection for groundwater model reduction using proper orthogonal decomposition. Water Resour. Res. 46. https://doi.org/10.1029/2009WR008792, n/a-n/a.

Stanko, Z.P., Boyce, S.E., Yeh, W.W.-G., 2016. Nonlinear model reduction of unconfined groundwater flow using POD and DEIM. Adv. Water Resour. 97, 130–143. https://doi.org/10.1016/j.advwatres.2016.09.005.

Ştefănescu, R., Navon, I.M., 2013. POD/DEIM nonlinear model order reduction of an ADI implicit shallow water equations model. J. Comput. Phys. 237, 95–114. https://doi.org/10.1016/j.jcp.2012.11.035.

Tezduyar, T.E., Sathe, S., Schwaab, M., Conklin, B.S., 2008. Arterial fluid mechanics modeling with the stabilized space – time fluid – structure interaction technique. Int. J. Numer. Methods Fluids 601–629. https://doi.org/10.1002/fld.

Vermeulen, P.T.M., Heemink, A.W., te Stroet, C.B.M., 2004a. Low-dimensional modelling of numerical groundwater flow. Hydrol. Process. 18, 1487–1504. https://doi.org/10.1002/hyp.1424.

Vermeulen, P.T.M., Heemink, A.W., Te Stroet, C.B.M., 2004b. Reduced models for linear groundwater flow models using empirical orthogonal functions. Adv. Water Resour. 27, 57–69. https://doi.org/10.1016/j.advwatres.2003.09.008.

White, J.T., Fienen, M.N., Doherty, J.E., 2016. A python framework for environmental model uncertainty analysis. Environ. Model. Softw. 85, 217–228. https://doi.org/10.1016/j.envsoft.2016.08.017.

Xiao, D., Fang, F., Buchan, A.G., Pain, C.C., Navon, I.M., Du, J., Hu, G., 2014. Non-linear model reduction for the Navier–Stokes equations using residual DEIM method. J. Comput. Phys. 263, 1–18. https://doi.org/10.1016/j.jcp.2014.01.011.

Zheng, C., 2009. Recent developments and future directions for MT3DMS and related transport codes. Ground Water 47, 620–625. https://doi.org/10.1111/j.1745-6584.2009.00602.x.

Zheng, C., Bennett, G.D., 2002. Applied Contaminant Transport Modeling, 2nd ed. Wiley-Interscience, New York.

Zheng, C., Wang, P.P., 1999. MT3DMS: aA Modular Three-Dimensional Multispecies Transport Model for simulation of advection, dispersion and chemical reactions of contaminants in groundwater systems. A Modul. three-dimensional multi-species … 239.

4 Conclusion

4.1 Reduced Nonlinear Groundwater Flow

For nonlinear groundwater flow, model reduction with POD and DEIM was successfully applied to both 1D and 2D test problems. The nonlinear model reduction was applied to unconfined groundwater flow and implemented within the MODFLOW-OWHM software, which allows for versatile future improvements and applications. The 1D test problem demonstrates the POD-DEIM algorithm's effectiveness by reducing the problem dimensions from 200 to 5 with trivial errors. In the more complex 2D test problem, the POD-DEIM algorithm reduced the problem dimensions from 39,204 to 250 and obtained a good solution with acceptable error. Generally, the full model was approximated very well at most times and locations. Maximum errors, which occurred in some isolated regions between interpolation points, were shown stabilize as simulation time advance and never exceeded an acceptable threshold. The reduced models can be developed to minimize error at certain times and locations of interest by modifying the snapshot selection. Overall, this demonstration of good reduced model performance, even without any optimal snapshot selection, is promising for the future application of POD-DEIM to more complex unconfined groundwater flow models.

4.2 Reduced Nonlinear Solute Transport

For nonlinear solute transport, model reduction with POD and DEIM was also successful. Nonlinear sorption was simulated, and this model reduction was performed within the recently released MT3D-USGS software. Similarly, a 1D test problem was first used to demonstrate that the new proposed method could reproduce a simple full model solution with trivial errors. The

dimension reduction for the 1D test problem was from 100 to 42, which suggested the potential for reduction with POD-DEIM might be more limited when applied to solute transport. The 2D test problem did exhibit significant dimension reduction from 13,248 to 286 and reproduced the full model solute plume with maximum errors less than 2% of the concentrations being simulated. The number of interpolation points (i.e., the size of the reduced dimension) needed for the reduced model was investigated and the extent of dimension reduction could be dependent on the fractional area of the model domain experiencing substantive changes in concentration. Since the solute plume in the 2D problem occupied a smaller fraction of the overall model domain than in the 1D problem, the degree of dimension reduction was larger. Both the 1D and 2D problems showed high sensitivity of the reduced model error to both the POD and DEIM reduced dimensions as well as to the snapshot selection. Generally, POD-DEIM performed well for nonlinear solute transport once a "sweet spot" was found with the reduced dimensions and snapshot set.

4.3 Overall Conclusions

Considering the successes of both applications of POD-DEIM, there is good evidence that the new method could be applied to a wide range of problems. The test cases presented were designed such that they had sufficient complexity to demonstrate the method's performance on difficult problems, while also having manageable runtimes to perform many computational experiments. Given a "real world" application, and an appropriate snapshot selection strategy, the method should reduce the dimensions of the model substantially, thereby reducing the runtimes of each simulation and permitting any number of model runs within any kind of optimization or uncertainty analysis.

5 Future Research

There are two main areas of future research that are essential for the long-term viability of POD-based model reduction on groundwater flow and solute transport simulations. The first is the development of an optimal snapshot selection strategy and the second is the coupling of a reduced flow and a reduced transport model. There is also potential to further demonstrate the utility of these model reduction methods by applying them to larger, three-dimensional problems and by releasing the software as a formal package for MODFLOW-OWHM and MT3D-USGS.

5.1 Optimal Snapshot Selection

Primarily, the difficulty in obtaining a good reduced model solution with POD-DEIM lies in the snapshot selection strategy. Snapshot selection can be described as an experimental design problem where the "curse of dimensionality" exists because of an astronomical amount of possible snapshot sets. The snapshot selection process requires selecting the simulation times at which the full model solution is saved, the values of each stress applied to the model at each time, and the values of each parameter. Naturally, the more time steps, stresses, and parameters a model has, the larger the potential snapshot set. The snapshot set is usually constructed to capture the dynamics of the full model at a certain subset of the parameter space and/or a certain range of stresses. For this research, the snapshot set was always constructed via trial-and-error, and it often required lots of time to get one that performed well. This extra time could be thought of as adding to the "offline" time required to construct the reduce model. Without a method for automatically (or at least semi-automatically) finding a snapshot set for a given problem, the offline time can exceed the "online" time saved when running the reduced model instead of the full model.

Some research has been done to identify a snapshot selection algorithm (Siade et al., 2010) but not for nonlinear models and not for the combined POD and DEIM steps, where two snapshot sets are needed. One approach may be to use an evolutionary algorithm (or some other global search technique like particle swarm optimization) to search for an optimal snapshot set using heuristics. If a reasonable snapshot selection strategy were to be identified for model reduction with POD-DEIM, both the computational cost of constructing the reduced model offline and the computational benefit of running the reduced model online could be combined and compared to a full model alternative.

5.2 Coupled Flow and Transport

Solute transport within a groundwater simulation should adapt to any changes in the groundwater flow conditions. In this research, a steady groundwater flow field was used so that the POD-DEIM algorithm's implementation within the solute transport code could be isolated. Therefore, the transport simulations track a contaminant plume assuming the groundwater conditions are not changing. This is certainly an unrealistic assumption, but it is reasonable when considering the objective was to prove the concept of POD-DEIM applied to solute transport. For further practical applications of POD-DEIM in any real-world scenario, the groundwater flow model would be coupled to the solute transport model and both would be solved at each time step. The full model, in this case, could also have extra iterations at each time step to account for density dependence, like the software SEAWAT (Langevin et al., 2007). Future research is needed to investigate the interactions between a reduced groundwater flow model and a reduced solute transport model since it is not known how the errors might propagate. The potential for

computational savings would be much greater if POD-DEIM could be applied to both the flow and transport components of a single simulation.

5.3 More Complex Applications

A highlight for future potential would be the application of POD-DEIM to a large-scale, three-dimensional simulation. Most applications of model reduction to groundwater models are limited to two dimensions. These test problems may be sufficient to prove the concept of new methods but they do not go far enough to assess the practicality of the methods on a real-world problem. Many current groundwater modeling projects seek to simulate many complex processes in a large model domain over a long time horizon. These models can take hours, or days to run once. It would certainly be appealing if the proposed POD-DEIM approach would also work on such large-scale simulations. However, it would be a substantial effort to collect snapshots for these larger models in a way that doesn't exceed computational limitations. Likely, strategies from the two previously mentioned research topics would be needed. Additional novel methods in parallel computing may also be needed to store and process the larger snapshot sets. Despite these challenges, it is realistic to think they can be met with enhancements to POD-DEIM or a new generation of POD-based model reduction techniques.

5.4 Software packages

An advantage to the methods of this research is the implementation within commonly used software. MODFLOW-OWHM and MT3D-USGS both make use of the package framework, which means specific modeling features can be turned on or off by including or not including that package's input files. The model reduction code could be developed into formal packages for both MODFLOW-OWHM and MT3D-USGS. By creating a package, further research with

POD-DEIM will likely be made easier. The code would be accessible for anyone familiar with either of the modeling software and the optional model reduction package would be turned on just like any other package. Also, embedding POD-DEIM as a package within well-known software might enhance visibility for this research field. The model reduction code has already been designed to emulate existing packages; therefore, formalizing the code and releasing extended versions of MODFLOW-OWHM and MT3D-USGS is a logical next step.

5.5 References

Siade, A. J., M. Putti, and W. W.-G. Yeh (2010), Snapshot selection for groundwater model reduction using proper orthogonal decomposition, Water Resour. Res., 46, W08539, doi:10.1029/2009WR008792.

Langevin, C.D., Thorne, D.T., Jr., Dausman, A.M., Sukop, M.C., and Guo, Weixing (2007), SEAWAT Version 4: A Computer Program for Simulation of Multi-Species Solute and Heat Transport: U.S. Geological Survey Techniques and Methods Book 6, Chapter A22, 39 p.